Inorganic Chemistry

Article

pubs.acs.org/IC

Tunable Electrochemical and Catalytic Features of BIAN- and BIAO-Derived Ruthenium Complexes

Arijit Singha Hazari,[†] Ankita Das,[†] Ritwika Ray,[†] Hemlata Agarwala,[†] Somnath Maji,[†] Shaikh M. Mobin,[‡] and Goutam Kumar Lahiri*[,†]

[†]Department of Chemistry, Indian Institute of Technology Bombay, Powai, Mumbai 400076, India

[‡]Discipline of Chemistry, School of Basic Sciences, Indian Institute of Technology Indore, Indore 452017, India

Supporting Information

ABSTRACT: This article deals with a class of ruthenium−BIAN-derived complexes, $[Ru^{II}(tpm)(R\text{-}BIAN)Cl]ClO_4$ (tpm = tris(1-pyrazolyl)methane, R-BIAN = bis(arylimino)acenaphthene, R = 4-OMe ($[\mathbf{1a}]ClO_4$), 4-F ($[\mathbf{1b}]ClO_4$), 4-Cl ($[\mathbf{1c}]ClO_4$), 4-NO_2 ($[\mathbf{1d}]ClO_4$)) and $[Ru^{II}(tpm)(OMe\text{-}BIAN)\text{-}H_2O]^{2+}$ ($[\mathbf{3a}](ClO_4)_2$). The R-BIAN framework with R = H, however, leads to the selective formation of partially hydrolyzed BIAO ([*N*-(phenyl)imino]-acenapthenone)-derived complex $[Ru^{II}(tpm)(BIAO)Cl]ClO_4$ ($[\mathbf{2}]ClO_4$). The redox-sensitive bond parameters involving —N═C−C═N— or —N═C−C═O of BIAN or BIAO in the crystals of representative $[\mathbf{1a}]ClO_4$, $[\mathbf{3a}](PF_6)_2$, or $[\mathbf{2}]ClO_4$ establish its unreduced form. The chloro derivatives $\mathbf{1a}^+$−$\mathbf{1d}^+$ and $\mathbf{2}^+$ exhibit one oxidation and successive reduction processes in CH_3CN within the potential limit of ±2.0 V versus SCE, and the redox potentials follow the order $\mathbf{1a}^+ < \mathbf{1b}^+ < \mathbf{1c}^+ < \mathbf{1d}^+ \approx \mathbf{2}^+$. The electronic structural aspects of $\mathbf{1a}^n$−$\mathbf{1d}^n$ and $\mathbf{2}^n$ (n = +2, +1, 0, −1, −2, −3) have been assessed by UV−vis and EPR spectroelectrochemistry, DFT-calculated MO compositions, and Mulliken spin density distributions in paramagnetic intermediate states which reveal metal-based ($Ru^{II} \rightarrow Ru^{III}$) oxidation and primarily BIAN- or BIAO-based successive reduction processes. The aqua complex $\mathbf{3a}^{2+}$ undergoes two proton-coupled redox processes at 0.56 and 0.85 V versus SCE in phosphate buffer (pH 7) corresponding to $\{Ru^{II}\text{−}H_2O\}/\{Ru^{III}\text{−}OH\}$ and $\{Ru^{III}\text{−}OH\}/\{Ru^{IV}\text{═}O\}$, respectively. The chloro ($\mathbf{1a}^+$−$\mathbf{1d}^+$) and aqua ($\mathbf{3a}^{2+}$) derivatives are found to be equally active in functioning as efficient precatalysts toward the epoxidation of a wide variety of alkenes in the presence of $PhI(OAc)_2$ as oxidant in CH_2Cl_2 at 298 K, though the analogous $\mathbf{2}^+$ remains virtually inactive. The detailed experimental analysis with the representative precatalyst $\mathbf{1a}^+$ suggests the involvement of the active $\{Ru^{IV}\text{═}O\}$ species in the catalytic cycle, and the reaction proceeds through the radical mechanism, as also supported by the DFT calculations.

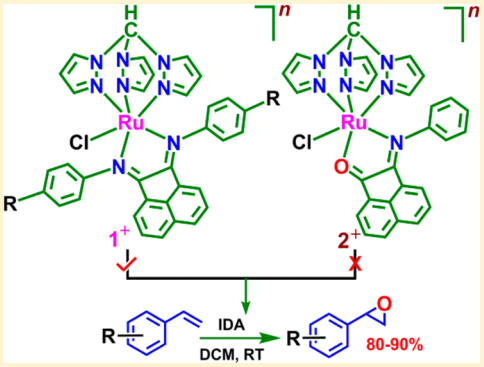

INTRODUCTION

The ruthenium complexes of α-diimine (—N═C−C═N—)-derived ligands have drawn significant attention over the decades primarily due to their diverse applications in dye-sensitized solar cells, molecular electronics, sensor technology, homogeneous catalysis, biomedical research, and supramolecular chemistry.[1] In this regard, metal complexes (main group as well as transition elements) of the robust framework of bis(arylimino)acenaphthene (BIAN) involving α-diimine fragment conjugated with the naphthalene ring (Chart 1) have recently been employed in catalysis and to understand other fundamental issues.[2] The corresponding ruthenium complexes of BIAN are however limited to a few recent reports,[3] dealing primarily with the structural and electronic aspects as well as their potential applications in catalysis.

The low-lying unoccupied molecular orbitals of BIAN, $\pi^*(\alpha$-diimine) (5b2) and π^*(naphthalene) (4a2), facilitate the successive electron uptake processes particularly on metalation, which in turn provides a multielectron reservoir platform suitable for selective application in catalysis.[3b−d,2m] The tetraanionic state of 1,2-bis[(2,6-diisopropylphenyl)imino]-acenaphthene has also been reported,[2n] involving the stepwise two-electron reductions of the α-diimine group followed by the addition of two more electrons over the multiple cation (Na^+) coordinated naphthalene π system.

The structural rigidity, stereoelectronic tunability based on the "R" groups (Chart 1), and facile successive electron-

Chart 1. Representation of R-BIAN and BIAO

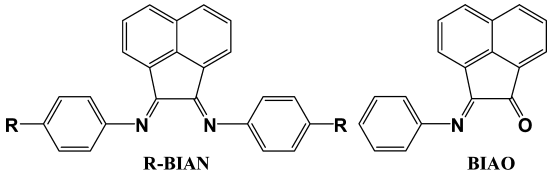

Received: March 18, 2015
Published: April 30, 2015

DOI: 10.1021/acs.inorgchem.5b00615
Inorg. Chem. 2015, 54, 4998−5012

Chart 2. Representation of Complexes

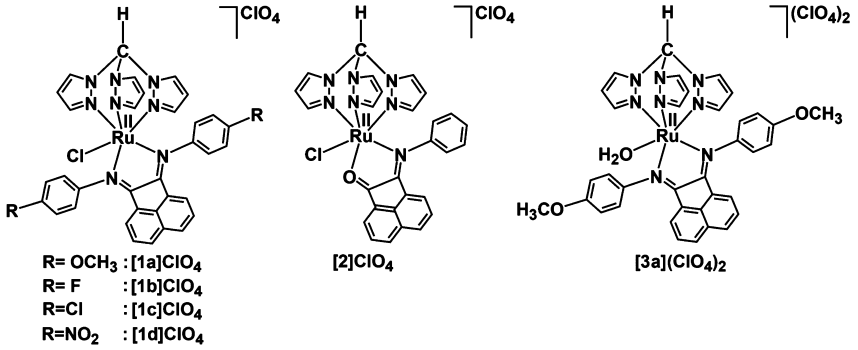

accepting feature of BIAN collectively make it an attractive ligand to design metal complexes suitable for electron-transfer processes and catalytic application.

In view of the aforestated unique features of BIAN, the present article is centered around the designing of ruthenium–BIAN-based complexes (Chart 2) of $[Ru^{II}(tpm)(R\text{-}BIAN)Cl]^+$ (tpm = tris(1-pyrazolyl)methane, R-BIAN = bis(arylimino)-acenaphthene, R = 4-OMe (**1a**$^+$), 4-F (**1b**$^+$), 4-Cl (**1c**$^+$), 4-NO_2 (**1d**$^+$)), $[Ru^{II}(tpm)(OMe\text{-}BIAN)H_2O]^{2+}$ (**3a**$^{2+}$), as well as partially in-situ-hydrolyzed BIAO for R = H (BIAO: [*N*-(phenyl)imino] acenapthenone) derived $[Ru^{II}(tpm)(BIAO)Cl]^+$ (**2**$^+$) with the broader perspectives of understanding their electronic structural aspects and catalytic potential.

Herein, we report the synthesis and characterization of $[\mathbf{1a}]ClO_4$–$[\mathbf{1d}]ClO_4$, $[\mathbf{2}]ClO_4$, and $[\mathbf{3a}](ClO_4)_2$, molecular structures of representative $[\mathbf{1a}]ClO_4$, $[\mathbf{2}]ClO_4$, and $[\mathbf{3a}](PF_6)_2$, and assessment of electronic structures of the chloro derivatives **1a**^{n}–**1d**^{n} and **2**^{n} (n = +2, +1, 0, −1, −2, −3) in accessible redox states via structure, UV–vis, and EPR spectroelectrochemistry in conjunction with DFT/TD-DFT calculations. The significant impact of "R" groups in the BIAN frameworks in **1a**$^+$–**1d**$^+$ and BIAO in **2**$^+$ on the redox processes has also been highlighted.

Further, the potential of **1a**$^+$–**1d**$^+$/**2**$^+$ or **3a**$^{2+}$ involving the labile Ru^{II}–Cl or Ru^{II}–OH_2 bond, respectively, as precatalyst for the epoxidation of a wide variety of alkenes has been explored with special references to (i) "R" groups in BIAN, (ii) $\{Ru^{II}–Cl\}$ versus $\{Ru^{II}–H_2O\}$, and (iii) BIAN versus BIAO. The limitation of the traditional method for epoxidation of alkenes by simple organic peracids involving the narrow substrate scope and inconvenience in product separation[4] has led to introduction of the metal complex-catalyzed efficient epoxidation process in the presence of suitable oxidants.[5] In this context, the initial report of Nishiyama et al. of ruthenium complex/TBHP (*tert*-butylhydroperoxide) catalyzed epoxidation of olefins in 1997[6] has spurred the subsequent utilization of varying ruthenium complexes in combination with suitable oxidants for the epoxidation reactions.[7]

RESULTS AND DISCUSSION

Synthesis, General Characterization, and Structure. The 1:1 electrolytic and diamagnetic complexes $[Ru^{II}(tpm)(R\text{-}BIAN)Cl]ClO_4$ (red powder) (tpm = tris(1-pyrazolyl)methane and BIAN = bis(arylimino)acenaphthene, R = 4-OMe $[\mathbf{1a}]ClO_4$, 4-F $[\mathbf{1b}]ClO_4$, 4-Cl $[\mathbf{1c}]ClO_4$, 4-NO_2 $[\mathbf{1d}]ClO_4$) have been prepared from the metal precursor $Ru^{III}(tpm)Cl_3$ in combination with respective R-BIAN in refluxing methanol under a dinitrogen atmosphere (Charts 1 and 2). The isolated perchlorate salts are purified by column chromatography on a neutral alumina column using 4:1 CH_2Cl_2–CH_3CN mixture as eluant. To our surprise, under identical reaction conditions the use of R-BIAN with R = H (Charts 1 and 2) selectively results in $[\mathbf{2}]ClO_4$ (blue powder) encompassing [*N*-(phenyl)imino]-acenapthenone (BIAO) via the hydrolysis of one of the imine bonds (—C═N—Ph → —C═O)[8] of BIAN. Complex **2**$^+$ represents the first example of a ruthenium-coordinated BIAO ligand; the corresponding mercury,[9] cobalt,[10] copper,[10] and zinc[11] complexes were however reported recently. The representative yellow-colored aqua derivative $[Ru^{II}(tpm)(4\text{-}OMe\text{-}BIAN)(H_2O)](ClO_4)_2$ $[\mathbf{3a}](ClO_4)_2$ (Chart 2) has been prepared from the corresponding chloro derivative ($[\mathbf{1a}]ClO_4$) in the presence of excess $AgClO_4$ in refluxing 1:3 acetone–water via the Cl/H_2O exchange process.[12,13]

The complexes exhibit satisfactory microanalytical data and molar conductivities in CH_3CN (Experimental Section). The ESI mass spectral data of $[\mathbf{1a}]ClO_4$-$[\mathbf{1d}]ClO_4$, $[\mathbf{2}]ClO_4$, and $[\mathbf{3a}](ClO_4)_2$ in CH_3CN and CH_3OH, respectively, match with their calculated values (Figure S1, Supporting Information and Experimental Section).

The molecular identities of the representative complexes $[\mathbf{1a}]ClO_4$, $[\mathbf{2}]ClO_4$, and $[\mathbf{3a}](PF_6)_2$ are authenticated by their single-crystal X-ray structures (Figures 1–3; Tables 1, 2, and S1, Supporting Information). We failed to generate suitable single crystal for $[\mathbf{3a}](ClO_4)_2$; however, the corresponding $[\mathbf{3a}](PF_6)_2$ results in a single crystal suitable for its structure

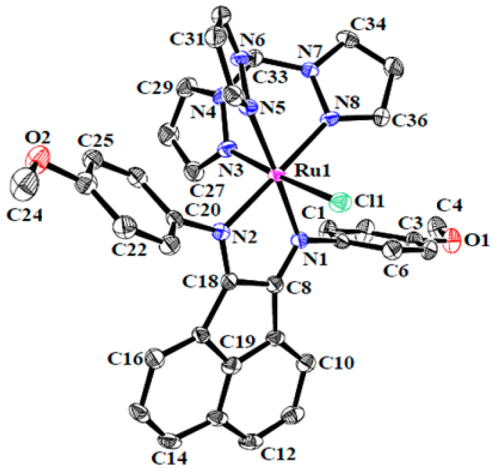

Figure 1. ORTEP[14] diagram of the cationic part of $[\mathbf{1a}]ClO_4 \cdot 2CH_2Cl_2$. Ellipsoids are drawn at the 50% probability level. ClO_4^- anion, hydrogen atoms, and solvent molecules are omitted for clarity.

DOI: 10.1021/acs.inorgchem.5b00615
Inorg. Chem. 2015, 54, 4998–5012

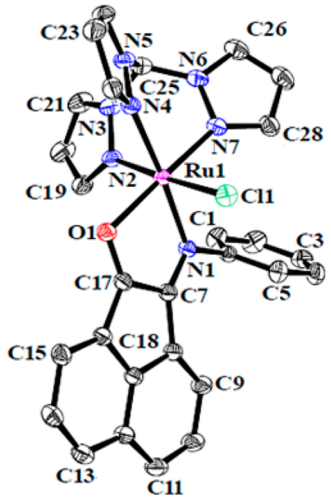

Figure 2. ORTEP[14] diagram of the cationic part of [**2**]ClO_4. Ellipsoids are drawn at the 40% probability level. ClO_4^- anion and hydrogen atoms are omitted for clarity.

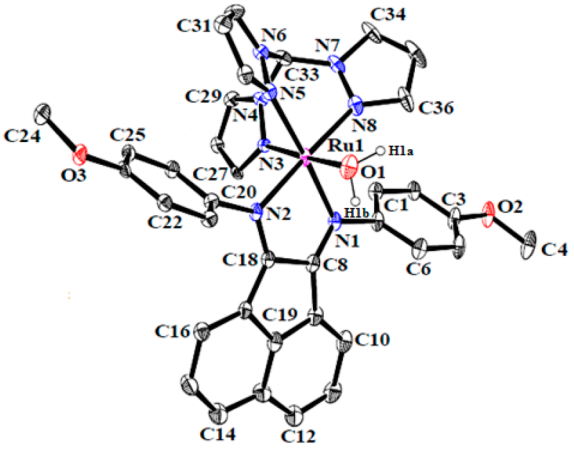

Figure 3. ORTEP[14] diagram of the dicationic part of [**3a**]$(PF_6)_2$·C_3H_6O. Ellipsoids are drawn at the 40% probability level. PF_6^- anions, hydrogen atoms, and solvent molecule are omitted for clarity.

determination. The tridentate tpm ligand is bonded to the metal ion in [**1a**]ClO_4 or [**2**]ClO_4 or [**3a**]$(PF_6)_2$ through its pyrazolyl nitrogen donors in the usual facial mode, resulting in two shared six-membered chelates.[13] The N,N or N,O donors of BIAN or BIAO in [**1a**]ClO_4/[**3a**]$(PF_6)_2$ or [**2**]ClO_4, respectively, form a five-membered chelate with the metal ion. The bite angles of the six-membered chelates involving the tpm ligand, N3−Ru1−N5 (86.37(10)°)/N5−Ru1−N8 (83.87(9)°), N2−Ru1−N4 (85.16(9)°)/N4−Ru1−N7 (85.73(9)°), and N3−Ru1−N5 (85.86 (15)°)/N5−Ru1−N8 (83.49(17)°), are appreciably larger than those of the corresponding five-membered chelates involving BIAN, N1−Ru1−N2 (79.08(10)°) in [**1a**]ClO_4, N1−Ru1−N2 (78.59(16)°) in [**3a**]$(PF_6)_2$ or BIAO, and N1−Ru1−O1 (80.14(8)°) in [**2**]ClO_4 (Table S1, Supporting Information). This in conjunction with the smaller average trans angles, 176.60°, 176.91°, and 176.71° in [**1a**]ClO_4, [**2**]ClO_4, and [**3a**]$(PF_6)_2$, respectively (Table S1, Supporting Information), suggest distorted octahedral geometries.

The Ru^{II}−N(tpm),[13] Ru^{II}−N(BIAN),[3a−c] Ru^{II}−Cl,[13a,b,15] and Ru^{II}−O(H_2O)[13a,b,16] bond lengths in [**1a**]ClO_4, [**2**]ClO_4, and [**3a**]$(PF_6)_2$ match fairly well with those of the reported analogous systems.

The feasibility of accepting successive two electrons by the low-lying π^* orbitals of the conjugated —N═C−C═N— (α-diimine) or —N═C−C═O (α-ketoimine) fragment of BIAN or BIAO, respectively, leads to the three redox states, fully oxidized neutral form (**A**) to intermediate one-electron reduced radical state (**B**) to doubly reduced dianionic form (**C**) (Scheme 1) with distinctive C−N (1.30, 1.35, 1.38 Å), C−O (1.25, 1.28, 1.31 Å), and C−C (≥1.47, ∼1.43, ∼1.38 Å) bond distances, respectively.[3a−c] The experimentally observed single-bond C−C length [C8−C18 = 1.469(4) ([**1a**]ClO_4) and 1.476(7) Å ([**3a**]$(PF_6)_2$), C7−C17 = 1.474(4) Å ([**2**]ClO_4)] and double bond C−N length [C8−N1/C18−N2 = 1.298(4)/1.307(3) ([**1a**]ClO_4) and 1.291(6)/1.299(6) Å ([**3a**]$(PF_6)_2$) and C7−N1/C17−O1 1.303(3)/1.249(3) Å ([**2**]ClO_4)], however, unequivocally establish that the unreduced form of BIAN or BIAO links to the ruthenium(II) ion in the complexes.

The calculated bond parameters of $\mathbf{1a}^+$−$\mathbf{1d}^+$, $\mathbf{2}^+$, and $\mathbf{3a}^{2+}$ based on their DFT-optimized structures (B3LYP-LANL2DZ/SDD basis set) in the singlet ground state (S = 0) (Table 2 and Tables S2−S11, Figure S2, Supporting Information) match fairly well with the X-ray data of representative complexes.

The IR spectra (KBr pellets) of [**1a**]ClO_4−[**1d**]ClO_4, [**2**]ClO_4, and [**3a**]$(ClO_4)_2$ display characteristic strong ClO_4^- vibrations at around 1100 and 625 cm^{-1},[3a] the C═O vibration of [**2**]ClO_4 at 1690 cm^{-1},[17] and OH vibration of [**3a**]$(ClO_4)_2$ at 3438 cm^{-1} [13a] (Experimental Section).

^{1}H NMR spectra of $\mathbf{1a}^+$−$\mathbf{1d}^+$ and $\mathbf{2}^+$ in $CDCl_3$ (Figures 4 and S3, Supporting Information and Experimental Section) and $\mathbf{3a}^{2+}$ in D_2O (Figure 4) display partially overlapping calculated number of aromatic proton resonances (tpm = 9, BIAN = 14, BIAO = 11) within the chemical shift range δ 6−9 ppm. The slightly acidic CH proton resonance of tpm for $\mathbf{1a}^+$−$\mathbf{1d}^+$ or $\mathbf{2}^+$ appears at a sharp and moderately strong singlet at δ ∼10 ppm;[13] however, the same for $\mathbf{3a}^{2+}$ in D_2O resolves as a weak but distinct peak at δ 9.7 ppm. The proton resonances associated with the six-membered rings of BIAN or BIAO in $\mathbf{1a}^+$−$\mathbf{1d}^+$/$\mathbf{3a}^{2+}$ or $\mathbf{2}^+$, respectively, can easily be distinguished from those of the five-membered rings of tpm, primarily based on their difference in spin−spin coupling constant (J/Hz) values (7−8 for BIAN or BIAO and 2−3 for tpm).[3a,13] The OMe signal for $\mathbf{1a}^+$ or $\mathbf{3a}^{2+}$ appears at δ/ppm 3.80 or 3.79, respectively. The variation of chemical shift values based on the substituents at the BIAN framework in $\mathbf{1a}^+$−$\mathbf{1d}^+$ is rather insignificant.

Electrochemistry, MO Composition, and Spin Density Distribution. The chloro derivatives $\mathbf{1a}^+$−$\mathbf{1c}^+$ and $\mathbf{2}^+$ exhibit similar electrochemical features with one oxidation (O1) and two successive reductions (R1 and R2), while complex $\mathbf{1d}^+$ incorporating *para*-NO_2-substituted BIAN (Chart 2) possesses one oxidation (O1) and four reductions (R1−R4) in CH_3CN within the potential window of ±2.0 V versus SCE (Figure 5, Table 3).

The redox potentials of $\mathbf{1a}^+$−$\mathbf{1d}^+$ vary systematically depending on the electron-donating or -withdrawing effect of the substituents in the BIAN framework, and it follows the order $\mathbf{1a}^+$ < $\mathbf{1b}^+$ < $\mathbf{1c}^+$ < $\mathbf{1d}^+$. The impact of the —N═C−C═O chromophore of BIAO in $\mathbf{2}^+$ with regard to the —N═C−C═N— fragment of BIAN in analogous $\mathbf{1a}^+$−$\mathbf{1d}^+$ has been reflected in its relatively higher oxidation potential (0.93 V), even comparable to that of the *para*-NO_2-substituted BIAN in $\mathbf{1d}^+$ (0.94 V).

DOI: 10.1021/acs.inorgchem.5b00615
Inorg. Chem. 2015, 54, 4998−5012

Table 1. Selected Crystallographic Data for [1a]ClO_4, [2]ClO_4, and [3a]$(PF_6)_2$

	[1a]ClO_4·$2CH_2Cl_2$	[2]ClO_4	[3a]$(PF_6)_2$·C_3H_6O
empirical formula	$C_{38}H_{34}Cl_6N_8O_6Ru$	$C_{28}H_{21}Cl_2N_7O_5Ru$	$C_{39}H_{38}N_8O_4F_{12}P_2Ru$
fw	1012.50	707.49	1073.78
cryst syst	monoclinic	monoclinic	triclinic
space group	$P2_1/n$	$P2_1/c$	P-1
a (Å)	11.7233 (3)	14.48414 (14)	11.650 (2)
b (Å)	17.2500 (4)	12.64471 (11)	14.944 (3)
c (Å)	20.1702 (5)	15.76167 (15)	16.267 (3)
α (deg)	90	90	71.09 (3)
β (deg)	94.8260 (10)	92.8914 (9)	69.90 (3)
γ (deg)	90	90	72.02 (3)
V (Å^3)	4064.50 (17)	2883.04 (5)	2453.3 (9)
Z	4	13	2
μ (mm^{-1})	0.838	6.554	0.476
T (K)	100 (2)	150 (2)	100 (2)
D_{calcd} (g cm^{-3})	1.655	1.630	1.454
F(000)	2048	1424	1084
θ range (deg)	1.55−29.78	3.05−72.16	1.48−24.29
data/restraints/params	11 546/0/534	5627/0/388	7908/1/607
R1, wR2 [$I > 2\sigma(I)$]	0.0520, 0.1223	0.0357, 0.1031	0.0584, 0.1396
R1, wR2(all data)	0.0776, 0.1368	0.0376, 0.1058	0.0864, 0.1508
GOF	1.048	1.057	1.001
largest diff. peak/hole (e Å^{-3})	1.60/−1.06	0.56/−0.51	1.18/−0.71

Table 2. Experimental and DFT-Calculated Selected Bond Lengths (Angstroms) for [1a]ClO_4, [2]ClO_4, and [3a]$(PF_6)_2$

	[1a]ClO_4		[2]ClO_4		[3a]$(PF_6)_2$	
	X-ray	DFT	X-ray	DFT	X-ray	DFT
Ru1−N1	2.021(2)	2.088	2.020(2)	2.077	2.038(4)	2.104
Ru1−N2	2.033(2)	2.087	2.057(2)	2.112	2.036(4)	2.116
Ru1−N3	2.047(3)	2.118			2.023(4)	2.070
Ru1−N4			2.068(2)	2.095		
Ru1−N5	2.070(2)	2.127			2.075(4)	2.147
Ru1−N7			2.042(2)	2.071		
Ru1−N8	2.083(2)	2.129			2.060(5)	2.133
Ru1−O1			2.0818(19)	2.108	2.126(4)	2.218
Ru1−Cl1	2.3965(8)	2.430	2.3690(7)	2.391		
C8−N1	1.298(4)	1.302			1.291(6)	1.303
C18−N2	1.307(3)	1.302			1.299(6)	1.306
C7−C17			1.474(4)	1.490		
C8−C18	1.469(4)	1.483			1.476(7)	1.495
C17−O1			1.249(3)	1.252		
C6−N1			1.443(3)	1.428		
C7−N1	1.445(4)	1.428	1.303(3)	1.307	1.446(6)	1.430
C20−N2	1.430(4)	1.428			1.419(6)	1.431

Scheme 1. Varying Redox States of BIAN and BIAO

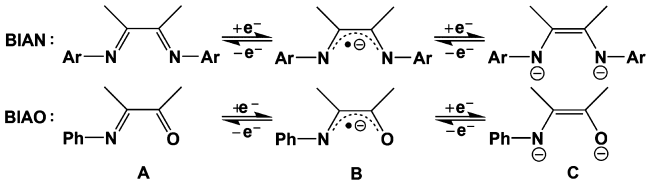

The origin of the redox processes of $\mathbf{1a}^+$−$\mathbf{1d}^+$ and $\mathbf{2}^+$ (Figure 5, Table 3) has been ascertained via the DFT-calculated MO compositions (Tables 4 and S12−S34, Supporting Information) and Mulliken spin density distributions (Table 5 and Figure 6) in paramagnetic intermediate states. The metal-based HOMO of $\mathbf{1a}^+$−$\mathbf{1d}^+$/$\mathbf{2}^+$ in the S = 0 state (∼60%) and β-LUMO of $\mathbf{1a}^{2+}$−$\mathbf{1d}^{2+}$/$\mathbf{2}^{2+}$ in the S = 1/2 state (>60%) as well as metal-dominated spin (>0.75) collectively suggest the correspondences of O1 to a $Ru^{II} \rightarrow Ru^{III}$ oxidation process. In consequence, the redox-sensitive C−C, C−N, and C−O bond distances of BIAN and BIAO remain virtually invariant on the oxidation process (O1) (Scheme 1, Tables 6 and S2, S4, S6, S8, and S10, Supporting Information). The metal-based oxidation process has been further evidenced by the highly anisotropic EPR spectrum of coulometrically oxidized representative $\mathbf{1a}^{2+}$ with g_1 = 2.674, g_2 = 2.212, g_3 = 1.769, Δg = 0.905, $\langle g \rangle$ = 2.248 ($\Delta g = g_1 - g_3$ and $\langle g \rangle = \{1/3(g_1^2 + g_2^2 + g_3^2)\}^{1/2}$) (Figure 7a).[22]

It should be noted that an appreciable contribution of Cl in the HOMO of $\mathbf{1a}^+$−$\mathbf{1d}^+$/$\mathbf{2}^+$ (>20%) and β-LUMO of $\mathbf{1a}^{2+}$−$\mathbf{1d}^{2+}$/$\mathbf{2}^{2+}$ (9−14%) has also been predicted due to the effect of Ru−Cl covalency. A similar sizable Cl contribution in the DFT-

DOI: 10.1021/acs.inorgchem.5b00615
Inorg. Chem. 2015, 54, 4998−5012

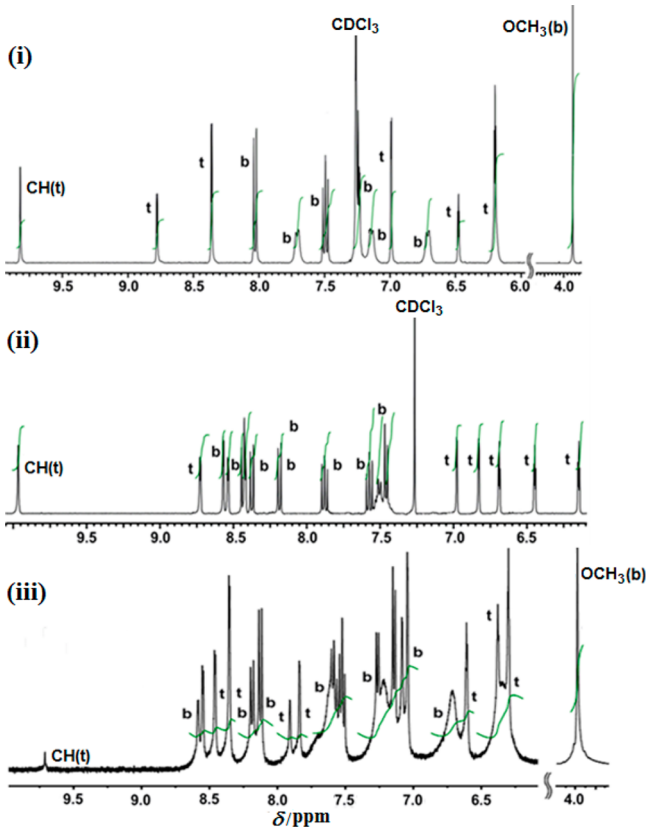

Figure 4. ^{1}H NMR spectra of (i) [**1a**]ClO_4, (ii) [**2**]ClO_4 in $CDCl_3$, and (iii) [**3a**]$(ClO_4)_2$ in D_2O (t = tpm, b = BIAN or BIAO).

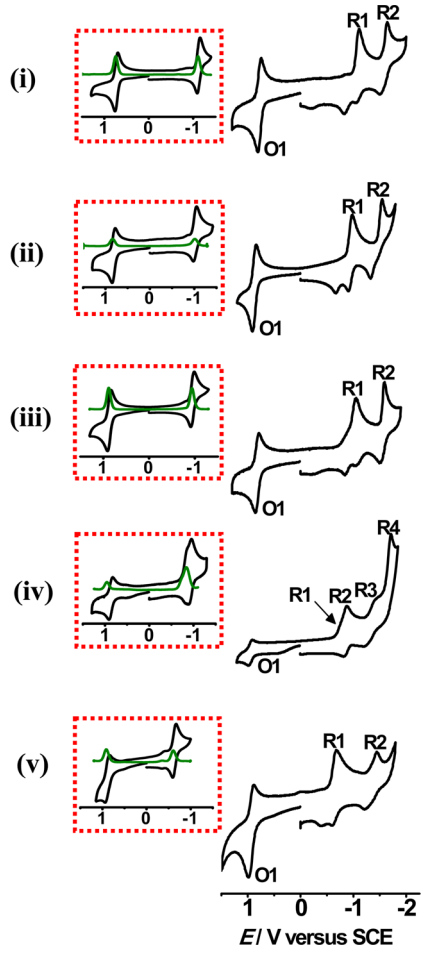

Figure 5. Cyclic voltammograms of (i) [**1a**]ClO_4, (ii) [**1b**]ClO_4, (iii) [**1c**]ClO_4, (iv) [**1d**]ClO_4, and (v) [**2**]ClO_4 in CH_3CN. (Inset) Cyclic voltammograms (black) and differential pulse voltammograms (green) of reversible oxidation (O1) and first reduction (R1) couples.

calculated MOs has also been pointed out earlier in analogous ruthenium complexes.[23]

The presence of two strong π-acceptor ligands, BIAN[3] and tpm,[13] in the complexes raises the pertinent question of their specific involvements in the successive reduction processes (Figure 5). The greater than 80% BIAN/BIAO contribution in the LUMO of **1a**$^+$−**1d**$^+$/**2**$^+$ (S = 0) and SOMO of **1a**−**1d**/**2** (S = 1/2) as well as —N═C−C═N— (BIAN)/—N═C−C═O (BIAO) dominated spin (>90%) (Table 4), however, supports the BIAN/BIAO-based first reduction process (R1 in Figure 5). This has been further supported by the free radical EPR with g = 2.001 (line width = 25 G) for the electrogenerated representative **2** (Figure 7b).[22] On the other hand, the mixed MO compositions of β-LUMO (BIAN/tpm, 50−60%/30−40%; BIAO/tpm, 69/25%) in **1a**−**1c** or **2** (S = 1/2) and HOMO (BIAN/tpm, 61−83%/10−37%; BIAO/tpm, 81/12%) in **1a**$^-$−**1c**$^-$ or **2**$^-$ (S = 0) suggest the partial involvement of tpm along with the BIAN- or BIAO-based orbitals in the second reduction process (R2 in Figure 5). On the contrary, the β-LUMO of **1d** (S = 1/2, BIAN, 96%) and HOMO of **1d**$^-$ (S = 0, BIAN 89%) imply solely a BIAN (—N═C−C═N— function) based second reduction (R2 in Figure 5). The involvement of BIAN (—N═C−C═N—) or BIAO (—N═C−C═O) in successive electron uptake processes (R1 and R2) finds further justification via the sequential shortening and lengthening of the DFT-calculated redox-sensitive C−C and C−N/C−O bond distances, respectively (Scheme 1, Table 6 and S2, S4, S6, S8, and S10, Supporting Information). The subsequent two reductions R3 and R4 of **1d**$^+$ in Figure 5 essentially involve the NO_2 group of BIAN (~95% BIAN contribution in LUMO of **1d**$^-$ (S = 0) and SOMO of **1d**$^{2-}$ (S = 1/2) as well as 98% BIAN-dominated spin in **1d**$^{2-}$) and a mixed tpm−BIAN-based situation, respectively (α-LUMO of **1d**$^{2-}$ (S = 1/2) = 88% tpm, SOMO of **1d**$^{3-}$ (S = 1) = 68% tpm/28% BIAN, and spin density of **1d**$^{3-}$ = BIAN(0.998)/tpm(0.951)).

Remarkably, the appreciable positive shift of the redox potential on selective incorporation of the electron-withdrawing NO_2 group in the BIAN framework in **1d**$^+$ (Table 3, Figure 5) facilitates detecting two additional reductions (R3 and R4) covering the NO_2 function/naphthalene ring of BIAN as well as the reduction of tpm as has been revealed by MO compositions and spin density plots.

The representative aqua derivative **3a**$^{2+}$ displays two successive one-electron oxidation processes, E°_{298},V (ΔE_p, mV) at 0.56(60) and 0.85(70) in phosphate buffer versus SCE at pH 7.0, which undergo anodic shifting with lowering pH (Figure S4, Table S35, Supporting Information), attributed to the simultaneous one-electron/one-proton transfer processes, leading to the {Ru^{IV}═O} state: Ru^{II}−OH_2/Ru^{III}−OH and Ru^{III}−OH/Ru^{IV}═O.[13a,24] Unfortunately, we failed to check the shift in potential of **3a**$^{2+}$ with the further change in pH primarily due to the associated precipitation problem.

The comparison of the oxidation potentials of the chloro (**1a**$^+$−**1d**$^+$, **2**$^+$) and aqua (**3a**$^{2+}$) derivatives with the reported analogous {Ru^{II}(tpm)(L)Cl} and {Ru^{II}(tpm)(L)H_2O} com-

DOI: 10.1021/acs.inorgchem.5b00615
Inorg. Chem. 2015, 54, 4998−5012

Table 3. Electrochemical Data[a]

complex	E°_{298}/V (ΔE_p/mV)[b] O1	O2	R1	R2	R3	R4	ref
			chloro derivatives				
[**1a**]ClO_4[c]	0.77(60)		−1.12(60)	−1.57(120)			this work
[**1b**]ClO_4[c]	0.82(60)		−1.01(70)	−1.54(70)			this work
[**1c**]ClO_4[c]	0.87(70)		−0.94(70)	−1.43(220)			this work
[**1d**]ClO_4[c]	0.94(60)		−0.77(60)	−0.85(60)	−1.31(180)	−1.71[d]	this work
[**2**]ClO_4[c]	0.93(90)		−0.62(70)	−1.32(230)			this work
$[Ru^{II}tpm(L^1)Cl]ClO_4$[c]	0.82						13a
$[Ru^{II}tpm(L^2)Cl]Cl$[c]	0.68						18
$[Ru^{II}tpm(L^3)Cl]Cl$[e]	0.65						19
$[Ru^{II}tpm(L^4)Cl]BF_4$[e]	0.83						20
$[Ru^{II}tpm(L^5)Cl]$[e]	0.24						20
$[Ru^{II}tpm(L^6)Cl]BF_4$[e]	0.79						13b
$[Ru^{II}tpm(L^7)Cl]$[e]	0.22						13b
$[Ru^{II}tpm(L^8)Cl]ClO_4$[c]	1.02						21
aqua derivatives							
[**3a**]$(ClO_4)_2$[f]	0.56(60)	0.85(70)					this work
$[Ru^{II}tpm(L^1)OH_2](ClO_4)_2$[g]	0.44	0.64					13a
$[Ru^{II}tpm(L^2)OH_2](ClO_4)_2$[h]	0.40	0.71					18
$[Ru^{II}tpm(L^3)OH_2](PF_6)_2$[I]	1.00						19
$[Ru^{II}tpm(L^4)OH_2](BF_4)_2$[j]	0.38						20
$[Ru^{II}tpm(L^5)OH_2]BF_4$[j]	0.17	0.37					20
$[Ru^{II}tpm(L^6)OH_2](PF_6)_2$[j]	0.38						13b
$[Ru^{II}tpm(L^7)OH_2]PF_6$[j]	0.16						13b

[a] L^1: *o*-benzoquinonediimine. L^2: 2,2′-bipyridine. L^3: 4-methyl-4′-(*N*-phenothiazylmethy1)-2,2′-bipyridine. L^4: 4,4′-dibenzyl-4,4′,5,5′-tetrahydro-2,2′-bioxazole. L^5: 2-[((1′*S*)-1′-(hydroxymethyl)-2′-phenyl)ethylcarboxamide]-(4*S*)-4-benzyl-4,5-dihydrooxazole. L^6: ((4*S*,4′*S*)-(−)-4,4′,5,5′-tetrahydro-4,4′-bis(1-methylethyl)-2,2′-bioxazole. L^7: *N*-(1-hydroxy-3-methylbutan-(2*S*)-(−)-2-yl)-(4*S*)-(−)-4-isopropyl-4,5-dihydrooxazole-2-carbimidate. L^8: 2-phenylazopyridine. [b] Potential in volts versus SCE; peak potential difference ΔE_p/mV (in parentheses). [c] In CH_3CN/0.1 M Et_4NClO_4 at 100 mV s^{-1}. [d] Irreversible. [e] In CH_3CN/0.1 M Bu_4NPF_6 at 100 mV s^{-1}. [f] In phosphate buffer, pH 7 at 100 mV s^{-1}. [g] In H_2O/0.1 M Et_4NClO_4, pH 7 at 100 mV s^{-1}. [h] In H_2O/0.1 M $NaCF_3SO_3$, pH 6.5 at 50 mV s^{-1}. [I] In CH_3CN/0.1 M Bu_4NPF_6, pH 7 at 100 mV s^{-1}. [j] In H_2O/0.1 M KCl, pH 7 at 100 mV s^{-1}.

plexes, respectively, integrating bidentate ligands (L) with different electronic properties (Table 3) reveals the significant variation in potential based on the π-accepting or σ-donating strength of L.

Spectroelectrochemistry and TD-DFT Calculations. The complexes (**1a**$^+$−**1d**$^+$ and **2**$^+$) exhibit a similar spectral profile in the UV−vis region in CH_3CN, and the transitions are assigned based on the TD-DFT calculations (Figure 8, Table 7). The moderately intense three visible bands in the range 700−400 nm are originated via BIAN/BIAO-targeted (dπ)Ru → (π*)BIAN/BIAO MLCT (metal-to-ligand charge transfer)[25] and (dπ)Ru/(π)BIAN/BIAO → (π*)BIAN/BIAO MLLCT (metal/ligand-to-ligand charge transfer)[25] transitions. The reversible one-electron oxidized species **1a**$^{2+}$−**1d**$^{2+}$ and **2**$^{2+}$ (O1, Figure 5) display two weak bands in the range 800−600 nm followed by an intense band near 400 nm, which are predicted to be originated via (π)BIAN/BIAO → (dπ)Ru LMCT (ligand-to-metal charge transfer) and (π)BIAN/BIAO/(dπ)Ru → (dπ)Ru LMLCT (ligand/metal-to-metal charge transfer) transitions. One-electron reversible reduction of **1a**$^+$−**1d**$^+$ to **1a**−**1d** (R1, Figure 5) causes the marginal change in band position as well as intensity of the BIAN-targeted MLCT or MLLCT band, though an appreciable change is noticed on moving from **2**$^+$ to **2**. The higher energy UV region bands in all cases are assigned to ligand-based ((π)BIAN/BIAO→(π*)BIAN/BIAO) transitions.

Catalytic Epoxidation. The accessibility of high-valent ruthenium−oxo {Ru^{IV}=O} species in the selective molecular frameworks has led to the exploration of their potential application in the catalytic epoxidation process.[7,13a,24a] In this context, the newly designed molecular sets **1a**$^+$−**1d**$^+$, **2**$^+$, and **3a**$^{2+}$ have been tested as possible precatalysts toward the epoxidation of a wide variety of alkenes. The initial standardization process has been monitored with the precatalyst **1a**$^+$ (chloro derivative) and styrene as the model substrate in combination with H_2O_2, TBHP, IDA, and *m*-CPBA (H_2O_2 = hydrogen peroxide, TBHP = *tert*-butyl hydrogen peroxide, IDA = iodobenzene diacetate, *m*-CPBA = *m*-chloroperbenzoic acid) as possible oxidants in CH_2Cl_2, CH_3CN, and C_2H_5OH solvents at 298 K (Table 8). The optimization study reveals that IDA and CH_2Cl_2 are the best oxidant and solvent, respectively, under the catalyst:substrate:oxidant molar ratio of 1:100:200, which gives maximum conversion of 88% (entry 4, Table 8). The above optimal condition (eq 1) with styrene as the model

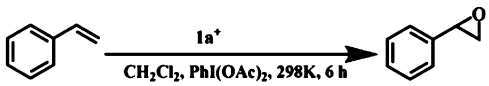

(1)

substrate has therefore been applied for the precatalysts **1a**$^+$−**1d**$^+$, which shows a marginal difference based on the electron-donating (OMe) or -withdrawing (NO_2, Cl, F) group at the para position of the arylimino moieties of BIAN. The representative aqua derivative **3a**$^{2+}$ extends comparable activity to that of **1a**$^+$ with selected tested alkenes (Table 9); therefore, the epoxidation reaction of a wide variety of alkenes has been performed selectively with **1a**$^+$. It should be noted that under the above reaction conditions (eq 1) no epoxide formation takes place in the absence of catalyst.

DOI: 10.1021/acs.inorgchem.5b00615
Inorg. Chem. 2015, 54, 4998−5012

Table 4. DFT-Calculated Selected MO Compositions of 1a″−1d″ and 2″

complex	MO	fragments	% contribution
$\mathbf{1a}^{+}$ (S = 0)	HOMO	Ru/Cl/BIAN/tpm	56/23/11/10
	LUMO	BIAN/Ru/tpm/Cl	82/11/06/01
$\mathbf{1a}^{2+}$ (S = 1/2)	β-LUMO	Ru/BIAN/tpm/Cl	61/20/09/09
1a (S = 1/2)	SOMO	BIAN/Ru/tpm/Cl	85/09/05/01
	β-LUMO	BIAN/tpm/Ru/Cl	55/40/04/01
$\mathbf{1a}^{-}$ (S = 0)	HOMO	BIAN/tpm/Ru	61/37/02
$\mathbf{1b}^{+}$ (S = 0)	HOMO	Ru/Cl/BIAN/tpm	59/23/09/09
	LUMO	BIAN/Ru/tpm/Cl	84/10/04/01
$\mathbf{1b}^{2+}$(S = 1/2)	β-LUMO	Ru/Cl/BIAN/tpm	67/13/10/10
1b (S = 1/2)	SOMO	BIAN/Ru/tpm/Cl	85/09/05/01
	β-LUMO	BIAN/tpm/Ru/Cl	54/41/04/01
$\mathbf{1b}^{-}$ (S = 0)	HOMO	BIAN/tpm/Ru/Cl	81/12/06/01
$\mathbf{1c}^{+}$ (S = 0)	HOMO	Ru/Cl/tpm/BIAN	60/23/09/09
	LUMO	BIAN/Ru/tpm/Cl	84/10/04/01
$\mathbf{1c}^{2+}$ (S = 1/2)	β-LUMO	Ru/Cl/BIAN/tpm	67/13/10/10
1c (S = 1/2)	SOMO	BIAN/Ru/tpm/Cl	85/09/05/01
	β-LUMO	BIAN/tpm/Ru/Cl	61/34/04/01
$\mathbf{1c}^{-}$ (S = 0)	HOMO	BIAN/tpm/Ru/Cl	83/10/06/01
$\mathbf{1d}^{+}$ (S = 0)	HOMO	Ru/Cl/tpm/BIAN	59/24/09/09
	LUMO	BIAN/Ru/tpm/Cl	86/09/03/01
$\mathbf{1d}^{2+}$ (S = 1/2)	β-LUMO	Ru/Cl/tpm/BIAN	67/13/10/09
1d (S = 1/2)	SOMO	BIAN/Ru/tpm/Cl	86/09/04/01
	β-LUMO	BIAN/Ru/tpm/Cl	96/02/01/00
$\mathbf{1d}^{-}$ (S = 0)	HOMO	BIAN/tpm/Ru/Cl	89/06/04/01
	LUMO	BIAN/Ru/tpm	95/03/02
$\mathbf{1d}^{2-}$ (S = 1/2)	SOMO	BIAN/Ru/tpm	94/03/02
	α-LUMO	tpm/Ru/BIAN	88/06/06
$\mathbf{1d}^{3-}$ (S = 1)	SOMO1	tpm/BIAN/Ru	68/28/04
$\mathbf{2}^{+}$ (S = 0)	HOMO	Ru/Cl/tpm/BIAO	60/24/11/05
	LUMO	BIAO/Ru/tpm/Cl	80/13/05/02
$\mathbf{2}^{2+}$ (S = 1/2)	β-LUMO	Ru/Cl/tpm/BIAO	68/14/11/06
2 (S = 1/2)	SOMO	BIAO/Ru/tpm/Cl	83/11/05/02
	β-LUMO	BIAO/tpm/Ru/Cl	69/25/05/01
$\mathbf{2}^{-}$ (S = 0)	HOMO	BIAO/tpm/Ru/Cl	81/12/06/01

Table 5. Mulliken Spin Densities for Paramagnetic Forms of 1a″−1d″ and 2″

complex	Ru	BIAN/BIAO	tpm	Cl
$\mathbf{1a}^{2+}$ (S = 1/2)	0.755	0.098	0.028	0.118
1a (S = 1/2)	0.047	0.941	0.010	0.004
$\mathbf{1b}^{2+}$ (S = 1/2)	0.782	0.032	0.062	0.147
1b (S = 1/2)	0.048	0.943	0.005	0.004
$\mathbf{1c}^{2+}$ (S = 1/2)	0.781	0.037	0.043	0.147
1c (S = 1/2)	0.049	1.001	0.010	0.005
$\mathbf{1d}^{2+}$ (S = 1/2)	0.777	0.035	0.036	0.152
1d (S = 1/2)	0.051	0.937	0.006	0.007
$\mathbf{1d}^{2-}$ (S = 1/2)	0.024	0.98	−0.001	−0.001
$\mathbf{1d}^{3-}$ (S = 1)	0.053	0.998	0.951	−0.002
$\mathbf{2}^{2+}$ (S = 1/2)	0.805	0.006	0.039	0.155
2 (S = 1/2)	0.040	0.946	0.008	0.005

Surprisingly, under identical reaction conditions (eq 1) the precatalyst $\mathbf{2}^{+}$ (chloro derivative) involving partially hydrolyzed BIAN ligand (i.e., BIAO) has failed to deliver any reasonable catalytic activities with any of the tested alkenes (Table 9). The observed inertness of $\mathbf{2}^{+}$ could possibly be attributed to its inability to form the necessary {Ru^{IV}═O} intermediate species (see below), as revealed by the independent reaction of $\mathbf{2}^{+}$ in CH_2Cl_2 or CH_3CN or C_2H_5OH with the oxidant (IDA or TBHP or H_2O_2 or *m*-CPBA).

Though the metal-catalyzed epoxidation process can also facilitate oxidative cleavage of the olefinic double bond resulting in aldehyde or ketone or alcohol,[26] the precatalyst $\mathbf{1a}^{+}$ or $\mathbf{3a}^{2+}$ is found to be chemoselective toward epoxide formation without any trace of carbonyl derivative as ascertained by GC-MS or ^{1}H NMR.

The efficiency of the catalyst $\mathbf{1a}^{+}$ has also been further tested by varying the catalyst loading with respect to the substrate vinyl cyclopentane, which gives an appreciably high TON of 2100 even with 0.001 mol % of the catalyst (Table S36, Supporting Information).

The individual role of the metal ion, the free ligand (tpm or BIAN), and the metal ion plus ligand toward the epoxidation process has been tested with vinyl cyclopentane under the reaction conditions in eq 1 (Table S37, Supporting Information), which divulges that Ru as $RuCl_3$ or free ligand (1:1 tpm-BIAN) or Ru as $RuCl_3$ + tpm (0.5:1 mol ratio) fails to facilitate the epoxidation process at all. However, Ru as $RuCl_3$ in combination with BIAN (0.5:1 mol ratio) yields slight conversion (18%) with moderate epoxide formation (30% selectivity). On the contrary, the infusion of free ligand (tpm + BIAN) and $RuCl_3$ in a 1:1 molar ratio (i.e., the in-situ-generated catalyst) enhances the yield up to 66% with 80% chemoselectivity, which is however less than that achieved by using the corresponding preformed catalyst $\mathbf{1a}^{+}$ (88% conversion, 100% selectivity, Table 9).

In general, complex $\mathbf{1a}^{+}$ is found to be an effective precatalyst for the oxidation of a wide variety of alkenes to respective epoxides under the standardized reaction conditions in eq 1, which gives excellent to good selectivity. It also reveals that unactivated olefins such as vinyl cyclohexane, 1-phenyl cyclohexene, vinyl cyclopentane, cyclooctene, cyclooctadiene, 1-octene, and 1-decene (entries 10−16, Table 9) exhibit comparable to better activity in terms of both % conversion and selectivity to that of aromatic alkenes. Though *cis*-stilbene and *trans*-stilbene (entries 7 and 8, Table 9) show chemoselective epoxidation to *cis*-stilbene oxide and *trans*-stilbene oxide, respectively, without any side product, α-methylstyrene (entry 2, Table 9) yields overoxidized acetophenone along with the desired epoxide as the primary product. The substrate cyclooctadiene yields the double epoxide as the main product (76%, entry 14, Table 9) with the partially oxidized monoepoxide minor product (8%). The controlled experiment comprising of 1:1 mixture of 1-octene and *trans*-5-decene as substrate reveals the preferential formation of terminal oxide (1,2-epoxyoctane, conversion 80%, selectivity 100%) over the internal oxide (1,2-epoxydecane, conversion 20%) (entry 17, Table 9).

As proposed earlier,[24] the ruthenium-catalyzed epoxidation reaction of alkene proceeds through the in situ formation of {Ru^{III}−OH} or {Ru^{IV}═O} active intermediate. The use of hydroxyl or radical scavenger specific for each intermediate, however, can distinguish between the nature of the active species.[27] The extent of variation in % conversion of the representative substrate 1-octene to its corresponding oxide in the presence of specific hydroxyl (*N*,*N*′-dimethylthiourea, DMTU) or radical (TEMPO, 2,2,6,6-tetramethylpiperidinyloxy radical) scavenger has thus been tested under similar reaction conditions (eq 1). Though the % conversion of 1-octene to its corresponding epoxide remains virtually unaltered in the presence of DMTU (Table S38, Supporting Information), the

DOI: 10.1021/acs.inorgchem.5b00615
Inorg. Chem. 2015, 54, 4998−5012

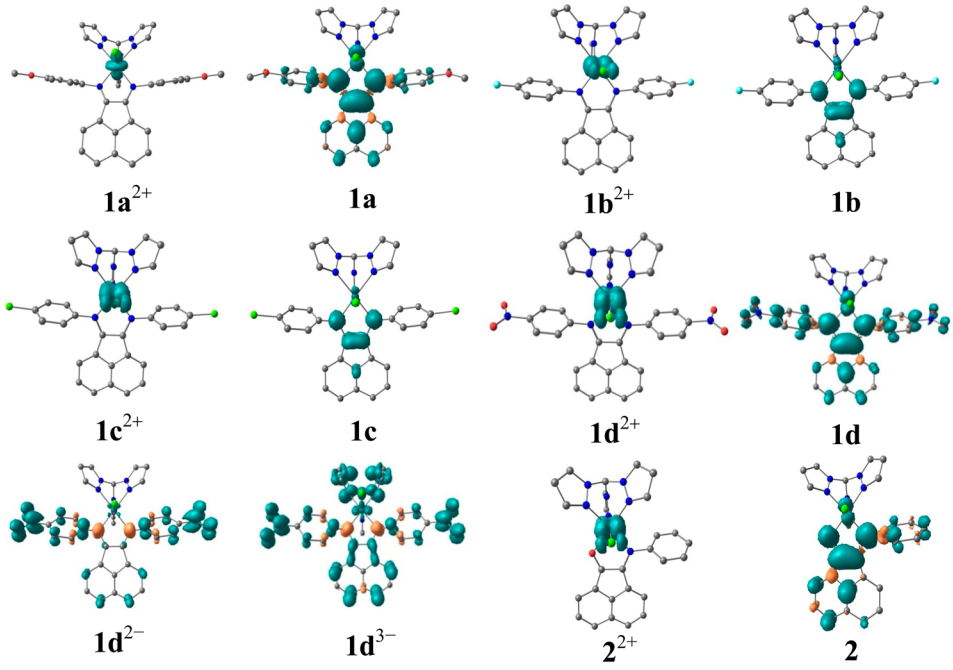

Figure 6. DFT-calculated Mulliken spin density plots of $\mathbf{1a}^{n}$−$\mathbf{1d}^{n}$ and $\mathbf{2}^{n}$.

Table 6. DFT(B3LYP/LANL2DZ/SDD)-Calculated Selected Bond Distances of Coordinated BIAN or BIAO in $\mathbf{1a}^{n}$−$\mathbf{1d}^{n}$ or $\mathbf{2}^{n}$

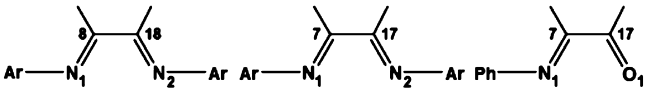

complex	C8–C18	C7–C17	N1–C8	N1–C7	N2–C18	N2–C17	O1–C17
$\mathbf{1a}^{2+}$	1.496		1.301		1.301		
$\mathbf{1a}^{+}$	1.483		1.302		1.302		
1a	1.431		1.339		1.340		
$\mathbf{1a}^{-}$	1.396		1.381		1.381		
$\mathbf{1b}^{2+}$		1.496		1.304		1.304	
$\mathbf{1b}^{+}$		1.484		1.301		1.301	
1b		1.431		1.340		1.340	
$\mathbf{1b}^{-}$		1.395		1.382		1.382	
$\mathbf{1c}^{2+}$		1.496		1.304		1.304	
$\mathbf{1c}^{+}$		1.484		1.301		1.301	
1c		1.431		1.340		1.341	
$\mathbf{1c}^{-}$		1.395		1.382		1.382	
$\mathbf{1d}^{2+}$		1.499		1.301		1.301	
$\mathbf{1d}^{+}$		1.485		1.301		1.301	
1d		1.434		1.340		1.339	
$\mathbf{1d}^{-}$		1.402		1.374		1.374	
$\mathbf{1d}^{2-}$		1.420		1.370		1.372	
$\mathbf{1d}^{3-}$		1.420		1.383		1.383	
$\mathbf{2}^{2+}$		1.508		1.303			1.257
$\mathbf{2}^{+}$		1.490		1.307			1.252
2		1.433		1.341			1.287
$\mathbf{2}^{-}$		1.395		1.396			1.314

complete inertness of alkene toward the epoxide formation on addition of TEMPO suggests the involvement of {Ru^{IV}=O} as an active intermediate (Scheme 2).

The formation of active {Ru^{IV}=O} intermediate has also been justified by the following controlled steps.

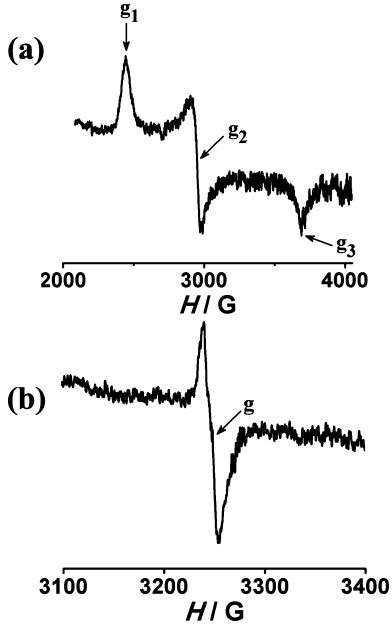

Figure 7. EPR spectra of electrogenerated (a) $\mathbf{1a}^{2+}$ and (b) **2** in CH_3CN/0.1 M Et_4NClO_4 at 77 K.

(1) Addition of IDA to a solution of precatalyst $\mathbf{1a}^{+}$ in CH_2Cl_2 immediately changes the color of the solution from red-brown to yellow due to the formation of {Ru^{IV}=O} species which causes the disappearance of the visible transitions of $\mathbf{1a}^{+}$ at 565 and 688 nm with the concomitant growth of two higher energy new bands at 482 and 430 nm (Figures S5 and S6, Supporting Information).[13a,24a,b] This has also been supported by the mass spectrometry which shows the peaks at m/z = 823.06 and 838.06 corresponding to {Ru^{IV}(tpm)(BIAN-O]ClO_4}$^{+}$ (calcd 823.20) ($\mathbf{4}^{2+}$) and {Ru^{II}(tpm)(BIAN-OCH_3}$^{+}$ (calcd 838.23), respectively (Figure S7, Supporting Information). The identification of the

DOI: 10.1021/acs.inorgchem.5b00615
Inorg. Chem. 2015, 54, 4998−5012

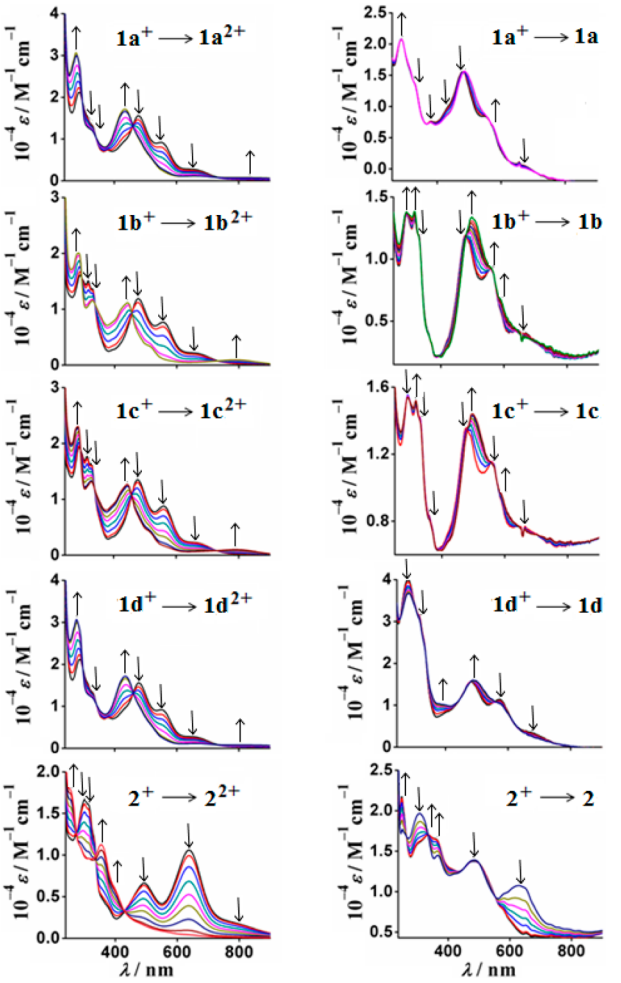

Figure 8. UV–vis spectroelectrochemical plots in CH_3CN/0.1 M NEt_4ClO_4.

solvated species ($\{Ru^{II}(tpm)(BIAN)OCH_3\}^+$) implies the reactive feature of the intermediate $\{Ru^{IV}{=}O\}$ species ($\mathbf{4}^{2+}$).

(2) The yellow solution of the intermediate $\mathbf{4}^{2+}$ reverts back to its original red-brown color ($\mathbf{1a}^+$) upon addition of Me_2S, which is attributed to the oxidation of dimethyl sulfide to dimethyl sulfoxide (GC) with the concomitant reduction of Ru(IV) to Ru(II) (Figure S5, Supporting Information).

(3) Addition of PPh_3 to the freshly prepared $\mathbf{4}^{2+}$ in $CDCl_3$ in a 1:1 ratio results in $Ph_3P{=}O$ as evidenced by its characteristic ^{31}P NMR resonance at δ 30 ppm (Figure S8, Supporting Information).[24a]

The olefin approaches the metal–oxo species either via side-on fashion or end-on fashion.[28] However, the observed appreciably higher % conversion in case of *trans*-stilbene (76%) as compared to *cis*-stilbene (66%) (entries 7 and 8, Table 9) suggests that the less hindered side-on approach is preferred. The probable five intermediates involving the transfer of oxygen of $\{M{=}O\}$ to the olefinic double bond are (a) concerted transition state, (b) radical, (c) carbocation, (d) π-radical cation, and (e) metallaoxetene[13a,24a,29] (Scheme 3).

The DFT calculations on the optimized adduct of ruthenium–oxo species ($\mathbf{4}^{2+}$, $\Delta E(S = 0)-(S = 1) = 7506$ cm^{-1}) with styrene as a model substrate i.e., [**5**] (Scheme 4 and Figure S9, Supporting Information), however, reveals the involvement of a radical intermediate step (**b** in Scheme 3) as it results in the lengthening of the $C_\alpha-C_\beta$ bond of styrene from 1.32 to1.50 Å in [**5**] with a simultaneous stretching of the Ru–O bond of 1.77 Å in $\mathbf{4}^{2+}$ to 1.93 Å in [**5**]. The formation of a C_β–O single bond (1.43 Å) in [**5**] leads to a radical center at C_α as has been corroborated by the Mulliken spin density of 0.76 on C_α. Moreover, the almost identical calculated Mulliken charge of 1.00 and 0.92 on Ru in optimized $\mathbf{4}^{2+}$ and [**5**], respectively, favors the radical mechanism (Schemes 2–4). The DFT-supported radical pathway can also be substantiated by the fact of no epoxide formation from 1-octene as a model substrate in the presence of radical scavenger TEMPO under the experimental conditions stated in eq 1.

CONCLUSION

In conclusion, the salient features of the article as well as the outlook are stated below.

- The newer classes of Ru–BIAN-derived chloro $[Ru^{II}(tpm)(R\text{-}BIAN)(Cl)]^+$ (R = 4-OMe, 4-F, 4-Cl, 4-NO_2, $\mathbf{1a}^+-\mathbf{1d}^+$) and aqua $[Ru^{II}(tpm)(OMe\text{-}BIAN)(H_2O)]^{2+}$ ($\mathbf{3a}^{2+}$) derivatives are reported. The BIAN framework with R = H, however, results in a partially hydrolyzed BIAO ([*N*-(phenyl)imino]acenapthenone)-derived first ruthenium complex $[Ru^{II}(tpm)(BIAO)(Cl)]^+$ ($\mathbf{2}^+$) (Chart 2).
- Appreciable variation in the redox potential based on the electronic nature of the "R" group of BIAN in $\mathbf{1a}^+-\mathbf{1d}^+$ or BIAO in $\mathbf{2}^+$ has been evident which in effect leads to the experimental observation of four successive reductions particularly in $\mathbf{1d}^+$ encompassing R = NO_2 group.
- The sensitivity of the —N=C–C=N— or —N=C–C=O bond parameters of BIAN or BIAO in accessible redox states of $\mathbf{1a}^n-\mathbf{1d}^n$ or $\mathbf{2}^n$ (n = +2, +1, 0, −1, −2, −3), respectively, has been reflected in experimental and DFT-optimized structures.
- The formation of the $\{Ru^{IV}{=}O\}$ state ($[Ru^{IV}(tpm)(R\text{-}BIAN)(O)]^{2+}$, $\mathbf{4}^{2+}$) for the BIAN-derived precursor chloro ($\mathbf{1a}^+-\mathbf{1d}^+$) or aqua ($\mathbf{3a}^{2+}$) derivative makes it an efficient precatalyst for the epoxidation of a wide variety of alkenes. The inaccessibility of the $\{Ru^{IV}{=}O\}$ state of the analogous BIAO-derived $\mathbf{2}^+$, however, makes it virtually ineffective for the epoxidation process.

The present article thus demonstrates enormous potential of the suitably designed BIAN-derived newer molecular frameworks toward the tunable electrochemical and catalytic applications.

EXPERIMENTAL SECTION

Materials. The ligands tris(1-pyrazolyl)methane (tpm)[30] and substituted bis(arylimino)acenaphthene (BIAN)[31] and the precursor complex $Ru(tpm)Cl_3{\cdot}1.5H_2O$[32] were prepared as reported previously in the literature. The starting material pyrazole was purchased from Sigma-Aldrich. Other solvents and reagents were of reagent grade and used as received. For spectroscopic and electrochemical studies, HPLC-grade solvents were employed.

Physical Measurements. The electrical conductivities of the complexes in CH_3CN were checked by using a Systronic 305 conductivity bridge. ^1H NMR and ^{31}P NMR spectra were recorded using Bruker Avance III 400 MHz. FT-IR spectra were recorded on a Nicolet spectrophotometer with samples prepared as KBr pellets. Cyclic voltammetry measurements were performed on a PAR model 273A electrochemistry system. Glassy carbon working electrode,

DOI: 10.1021/acs.inorgchem.5b00615
Inorg. Chem. 2015, 54, 4998–5012

Table 7. TD-DFT(B3LYP/CPCM/CH_3CN)-Calculated Electronic Transitions for 1a^n−1d^n and 2^n

λ/nm expt (DFT)	ε/M^{-1} cm^{-1} (f)	transitions	character
		1a^{2+} (S = 1/2)	
822(817)	810(0.039)	HOMO−2 → LUMO(98)	BIAN(π) → Ru(dπ)
660(614)	1170(0.004)	HOMO−4(β) → LUMO+1(β)(95)	BIAN(π) → Ru(dπ)
435(452)	17 150(0.052)	HOMO−10(β) → LUMO(β) (91)	BIAN(π) → Ru(dπ)
330(329)	11 890(0.073)	HOMO−2(β) → LUMO+2 (β) (64)	BIAN(π)/Ru(dπ) → BIAN(π*)
277(284)	30 670(0.004)	HOMO−6(β) → LUMO+2 (β)(64)	BIAN(π) → BIAN(π*)
		1a^{+} (S = 0)	
658(597)	2710(0.016)	HOMO → LUMO(61)	Ru(dπ) → BIAN(π*)
552(474)	9200(0.139)	HOMO−3 → LUMO(69)	Ru(dπ)/BIAN(π) → BIAN(π*)
478(448)	15 600(0.041)	HOMO−3 → LUMO(51)	Ru(dπ)/BIAN(π) → BIAN(π*)
379(370)	7360(0.022)	HOMO−3 → LUMO+1(69)	BIAN(π)/Ru(dπ) → BIAN(π*)
328(318)	13 350(0.231)	HOMO−5 → LUMO+1(66)	BIAN(π) → BIAN(π*)
288(261)	21 170(0.018)	HOMO−4 → LUMO+4(61)	BIAN(π) → BIAN(π*)
		1a (S = 1/2)	
658(648)	740(0.004)	HOMO(β) → LUMO(β)(98)	Ru(dπ) → BIAN(π*)
575(562)	6840(0.003)	HOMO−1(α) → LUMO(α)(58)	Ru(dπ) → BIAN(π*)
485(462)	15 680(0.223)	HOMO−1(α) → LUMO(α)(69)	Ru(dπ)/BIAN(π) → BIAN(π*)
379(378)	7470(0.040)	HOMO−4(β) → LUMO(β)(61)	BIAN(π) → BIAN(π*)
332(329)	13 360(0.002)	HOMO−4(β) → LUMO+1(β)(75)	BIAN(π) → BIAN(π*)
288(289)	20 820(0.013)	HOMO−3(β) → LUMO+3(β)(83)	BIAN(π) → BIAN(π*)/tpm(π*)
		1b^{2+} (S = 1/2)	
793(743)	950(0.017)	HOMO−2(β) → LUMO(β)(97)	BIAN(π) → Ru(dπ)
517(484)	3190(0.014)	HOMO−3(β) → LUMO+1(β)(62)	Ru(dπ) → BIAN(π*)
442(439)	11 210(0.050)	HOMO−2(β) → LUMO+1(β)(74)	BIAN(π) → BIAN(π*)
328(319)	11 560(0.004)	HOMO(α) → LUMO+2(α)(64)	BIAN(π) → BIAN(π*)
283(281)	20 070(0.013)	HOMO−6(β) → LUMO+2(β)(84)	BIAN(π) → BIAN(π*)
		1b^{+} (S = 0)	
662(590)	2140(0.022)	HOMO−1 → LUMO(55)	Ru(dπ) → BIAN(π*)
556(503)	7670(0.079)	HOMO−2 → LUMO(51)	Ru(dπ) → BIAN(π*)
476(441)	11 920(0.252)	HOMO → LUMO+1(62)	Ru(dπ) → BIAN(π*)
328(311)	13 660(0.006)	HOMO−4 → LUMO+1(52)	BIAN(π) → BIAN(π*)
314(307)	15 100(0.031)	HOMO−4 → LUMO+1(56)	BIAN(π)/Cl(π) → BIAN(π*)
289(273)	16 120(0.005)	HOMO−6 → LUMO+1(69)	BIAN(π)/Cl(π) → BIAN(π*)
		1b (S = 1/2)	
590(559)	6730(0.007)	HOMO−1(α) → LUMO(α)(52)	Ru(dπ) → BIAN(π*)
558(543)	9370(0.020)	HOMO−1(β) → LUMO(β)(82)	Ru(dπ) → BIAN(π*)
498(493)	13 360(0.004)	HOMO−2(β) → LUMO(β)(85)	Ru(dπ) → BIAN(π*)
331(352)	11 720(0.038)	HOMO−5(β) → LUMO(β)(82)	BIAN(π) → BIAN(π*)
316(306)	13 840(0.006)	HOMO−4(β) → LUMO+1(β)(68)	BIAN(π) → BIAN(π*)
291(294)	15 400(0.010)	HOMO−6(β) → LUMO(β)(68)	BIAN(π) → BIAN(π*)
		1c^{2+} (S = 1/2)	
796(741)	1050(0.014)	HOMO−2(β) → LUMO(β)(98)	BIAN(π) → Ru(dπ)
576(563)	1390(0.004)	HOMO−6(β) → LUMO(β)(82)	BIAN(π) → Ru(dπ)
521(515)	3840(0.022)	HOMO−8(β) → LUMO(β)(95)	BIAN(π) → Ru(dπ)
445(438)	12 700(0.063)	HOMO−2(β) → LUMO+1(β)(74)	BIAN(π)/Ru(dπ) → BIAN(π*)
329(323)	13 130(0.006)	HOMO−1(β) → LUMO+1(β)(91)	BIAN(π) → BIAN(π*)
286(266)	23 110(0.009)	HOMO−7(β) → LUMO+2(β)(87)	BIAN(π)/Cl(π) → BIAN(π*)
		1c^{+} (S = 0)	
664(593)	2250(0.024)	HOMO−1 → LUMO(55)	Ru(dπ)/BIAN(π) → BIAN(π*)
561(506)	8810(0.085)	HOMO−2 → LUMO(51)	Ru(dπ) → BIAN(π*)
477(441)	13 570(0.241)	HOMO → LUMO+1(51)	Ru(dπ) → BIAN(π*)
329(318)	16 340(0.039)	HOMO−9 → LUMO(67)	BIAN(π) → BIAN(π*)
315(307)	17 680(0.009)	HOMO−5 → LUMO+1(63)	BIAN(π) → BIAN(π*)
290(264)	19 270(0.001)	HOMO−7 → LUMO+1 (59)	BIAN(π) → BIAN(π*)
		1c (S = 1/2)	
590(567)	9440(0.049)	HOMO−1(β) → LUMO(β)(72)	Ru(dπ) → BIAN(π*)
564(504)	11 290(0.007)	HOMO−1(β) → LUMO(β)(79)	Ru(dπ) → BIAN(π*)
497(461)	14 410(0.051)	HOMO−1(α) → LUMO(α)(79)	Ru(dπ)/Cl(π) → BIAN(π*)
330(330)	13 990(0.008)	HOMO(β) → LUMO(β)(81)	Ru(dπ)/BIAN(π) → BIAN(π*)
317(311)	15 200(0.006)	HOMO−5(α) → LUMO(α)(61)	BIAN(π) → BIAN(π*)
291(279)	15 400(0.001)	HOMO−4(α) → LUMO+2(α)(79)	BIAN(π) → BIAN(π*)/tpm(π*)

DOI: 10.1021/acs.inorgchem.5b00615
Inorg. Chem. 2015, 54, 4998−5012

Table 7. continued

λ/nm expt (DFT)	ε/M^{-1} cm^{-1} (f)	transitions	character
		1d^{2+} (S = 1/2)	
827(879)	810(0.046)	HOMO(β) → LUMO(β) (98)	BIAN(π) → Ru(dπ)
657(594)	1140(0.001)	HOMO−6(β) → LUMO(β)(74)	BIAN(π) → Ru(dπ)
434(417)	17 200(0.030)	HOMO−3(β) → LUMO+1 (β)(74)	Ru(dπ) → BIAN(π*)
330(331)	11 950(0.002)	HOMO−9(β) → LUMO+1 (β)(51)	BIAN(π) → BIAN(π*)
277(274)	30 680(0.150)	HOMO−6(α) → LUMO+3 (α)(61)	BIAN(π) → BIAN(π*)
		1d^{+} (S = 0)	
652(595)	2780(0.028)	HOMO−1 → LUMO(50)	Ru(dπ) → BIAN(π*)
552(507)	9230(0.049)	HOMO → LUMO+1(54)	Ru(dπ) → BIAN(π*)
478(454)	15 570(0.028)	HOMO−1 → LUMO+1(66)	Ru(dπ) → BIAN(π*)
330(301)	13 230(0.099)	HOMO−4 → LUMO+1(52)	BIAN(π) → BIAN(π*)
287(281)	21 180(0.021)	HOMO−6 → LUMO+2(53)	BIAN(π)/Cl(π) → BIAN(π*)
		1d (S = 1/2)	
801(836)	1310(0.010)	HOMO(β) → LUMO(β) (96)	Ru(dπ) → BIAN(π*)
578(578)	10 260(0.002)	HOMO → 1(α)→LUMO+1(α)(77)	Ru(dπ) → BIAN(π*)
488(455)	16 010(0.009)	HOMO → 1(α)→LUMO+2(α)(59)	Ru(dπ) → BIAN(π*)
316(314)	30 580(0.005)	HOMO → 7(α)→LUMO(α)(58)	BIAN(π) → BIAN(π*)
283(295)	36 740(0.009)	HOMO−6(β) → LUMO(β)(62)	BIAN(π) → BIAN(π*)
		2^{2+} (S = 1/2)	
397(442)	6120(0.067)	HOMO−7(β) → LUMO (β)(88)	BIAO(π*) → Ru(dπ)
354(347)	11 270(0.048)	HOMO(α) → LUMO+1(α)(57)	BIAO(π) → BIAO(π*)
255(326)	17 860(0.001)	HOMO−2(α) → LUMO+1(α)(56)	BIAO(π) → BIAO(π*)
		2^{+} (S = 0)	
638(566)	10 550(0.170)	HOMO−2 → LUMO(47)	Ru(dπ) → BIAO(π*)
493(439)	6620(0.016)	HOMO−1 → LUMO+1(67)	Ru(dπ) → BIAO(π*)
378(372)	3630(0.006)	HOMO−5 → LUMO(68)	Cl(π)/BIAO(π) → BIAO(π*)
314(337)	16 090(0.013)	HOMO → LUMO+2(48)	Ru(dπ) → BIAO(π*)
301(305)	16 700(0.022)	HOMO−4 → LUMO+1(66)	BIAO(π)/Cl(π) → BIAO(π*)
		2 (S = 1/2)	
483(459)	13 700(0.001)	HOMO−2(α) → LUMO(α)(79)	Ru(dπ) → BIAO(π*)
362(365)	16 480(0.008)	HOMO−4(β) → LUMO(β)(62)	BIAO(π) → BIAO(π*)
337(326)	17 000(0.060)	HOMO−4(α) → LUMO(α)(54)	BIAO(π) → BIAO(π*)
249(317)	21 740(0.019)	HOMO−5(α) → LUMO(α)(38)	BIAO(π)/Cl(π) → BIAO(π*)
		HOMO−9(β) → LUMO(β)(37)	Cl(π)/BIAO(π) → BIAO(π*)

Table 8. Optimization of the Critical Reaction Parameters[a]

entry	solvent	catalyst **1a**$^{+}$ (mmol %)	oxidant	% conversion[b]
1	CH_2Cl_2	1	H_2O_2	22
2	CH_2Cl_2	1	TBHP	39
3	CH_2Cl_2	1	*m*-CPBA	27
4	CH_2Cl_2	1	IDA	88
5	CH_2Cl_2	0.5	IDA	75
6	CH_2Cl_2	2	IDA	88
7	C_2H_5OH	1	H_2O_2	27
8	C_2H_5OH	1	TBHP	32
9	C_2H_5OH	1	*m*-CPBA	19
10	C_2H_5OH	1	IDA	62
11	CH_3CN	1	H_2O_2	23
12	CH_3CN	1	TBHP	28
13	CH_3CN	1	*m*-CPBA	24
14	CH_3CN	1	IDA	68

[a]1 mmol of styrene, solvent = 3 mL, oxidant = 2 equiv, catalyst:substrate:oxidant = 1:100:200, 298 K, 6 h under aerobic conditions. [b]Percent (%) conversions were calculated by GC with *n*-decane as an internal standard as well as by GC-MS. TBHP: *tert*-butyl hydrogen peroxide. IDA: iodobenzene diacetate. *m*-CPBA: *m*-chloroperbenzoic acid. H_2O_2: hydrogen peroxide.

platinum wire auxiliary electrode, and a saturated calomel reference electrode (SCE) were used in a standard three-electrode configuration cell. A platinum wire-gauze working electrode was used for the constant potential coulometry experiment. UV−vis spectral studies were performed on a PerkinElmer Lambda 950 spectrophotometer. UV−vis spectroelectrochemical studies were performed on a BAS SEC2000 spectrometer system. The supporting electrolyte was Et_4NClO_4, and the solute concentration was $\sim 10^{-3}$ M. All electrochemical experiments were carried out under a dinitrogen atmosphere at 298 K. The half-wave potential E° was set equal to $0.5(E_{pa} + E_{pc})$, where E_{pa} and E_{pc} are anodic and cathodic cyclic voltammetry peak potentials, respectively. The elemental analyses were carried out on a Thermoquest (EA 1112) microanalyzer. Electrospray mass spectra (ESI-MS) were recorded on a Bruker's Maxis Impact (282001.00081). The EPR measurements were made with a JEOL model FA200 electron spin resonance spectrometer. GC analysis was done by a Shimadzu GC-2014 gas chromatograph with a FID detector using a capillary column (112−2562 CYCLODEXB, from J&W Scientific, length 60 m, inner diameter 0.25 mm, film 0.25 μm), and GC-MS analysis was performed on an Agilent Technologies 7890A GC system coupled with a 5975C inert XL EI/CI Mass Selective Detector (GCMSD) with its triple-axis detector.

Crystallography. Single crystals of [**1a**]ClO_4 and [**2**]ClO_4 were grown by slow evaporation of their 1:2 dichloromethane-*n*-hexane solutions, while those of [**3a**]$(PF_6)_2$ were obtained from 1:1 acetone-*n*-hexane solution. X-ray crystal data for [**1a**]ClO_4, [**2**]ClO_4, and [**3a**]$(PF_6)_2$ were collected on RIGAKU SATURN-724+, Agilent Technologies (Oxford Diffraction) SUPER NOVA, and Bruker SMART APEX-II, CCD diffractometers, respectively. The data collection for [**1a**]ClO_4 and [**2**]ClO_4 were evaluated using the

DOI: 10.1021/acs.inorgchem.5b00615
Inorg. Chem. 2015, 54, 4998−5012

Table 9. Catalytic Epoxidation of Olefins[a]

entry	substrate	product	%conversion (selectivity)[b]		
			$\mathbf{1a}^{+}$	$\mathbf{2}^{+}$	$\mathbf{3a}^{2+}$
1	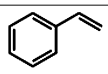	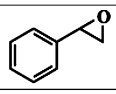	88(80)	10(50)	89(82)
2	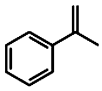	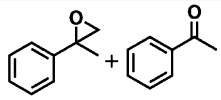	84(58+26)	0	NC
3	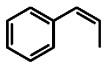	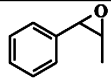	82(80)	0	NC
4	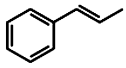	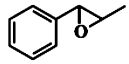	84(80)	0	NC
5	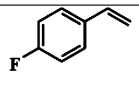	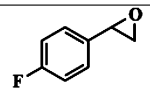	82(100)	0	NC
6	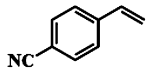	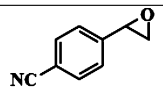	84(100)	18(10)	NC
7	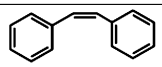	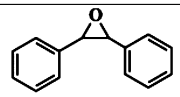	66(100)	0	70(80)
8	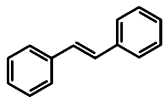	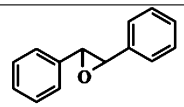	76(100)	12(10)	NC
9	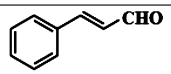	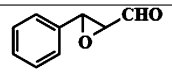	84(80)	18	NC
10	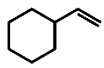	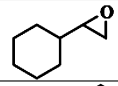	82(100)	0	NC
11	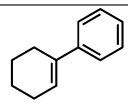	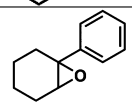	84(75)	0	NC
12	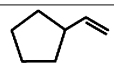	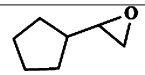	88(100)	0	NC
13			66(70)	0	NC
14		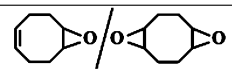	8/76(70)	12(0)	NC
15	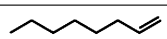	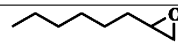	90(100)	25	92(100)
16	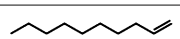	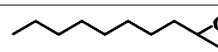	67(100)	0	NC
17	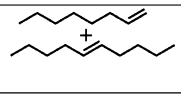	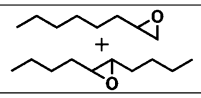	80(100) + 20	0	NC

[a]1 mmol of styrene, solvent = 3 mL, oxidant = 2 equiv, catalyst:substrate:oxidant = 1:100:200, 298 K, 6 h under aerobic conditions. Products are analyzed by GC with *n*-decane as an internal standard as well as by GC-MS. [b]Selectivity in terms of epoxide formation. NC = Not determined.

CrysAlisPro CCD and CrystalClear-SM Expert software, respectively. The data for $[\mathbf{1a}]ClO_4$ were collected by the standard $\phi-\omega$ scan techniques, scaled and reduced using CrysAlisPro RED software, and by the ω scan technique for $[\mathbf{2}]ClO_4$. The cell refinement and data reduction in $[\mathbf{3a}](PF_6)_2$ were performed with SAINT V7.68A. The structures were solved by direct method using SHELXS-97 and refined by full matrix least-squares with SHELXL-97, refining on F^2.[33] All non-hydrogen atoms were refined anisotropically. The hydrogen atoms were placed in geometrically constrained positions and refined with isotropic temperature factors, generally 1.2Ueq of their parent atoms. Except H1A and H1B (protons of aqua molecule in $[\mathbf{3a}](PF_6)_2$), the other hydrogen atoms were added in the refinement process as per the riding model. The disordered solvent molecules in $[\mathbf{1a}]ClO_4$ and $[\mathbf{3a}](PF_6)_2$ were SQUEEZED by the PLATON[34] program. CCDC 1052730 ($[\mathbf{1a}]ClO_4$), 1052731 ($[\mathbf{2}]ClO_4$), and 1052732 ($[\mathbf{3a}](PF_6)_2$) contain supplementary crystallographic data for this paper. These data can be obtained free of charge from The Cambridge Crystallographic Data Center via www.ccdc.cam.ac.uk/data_request/cis.

Computational Details. Full geometry optimizations were carried out by using the density functional theory method at the (R)B3LYP

DOI: 10.1021/acs.inorgchem.5b00615
Inorg. Chem. 2015, 54, 4998−5012

Scheme 2. Proposed Mechanistic Pathway

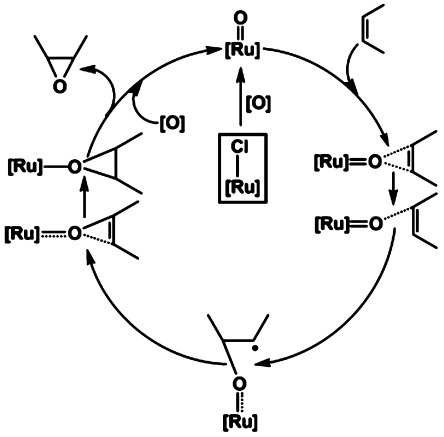

Scheme 3. Probable Intermediates in Metal-Catalyzed Oxygen Transfer Reaction from Metal−Oxo to Olefins

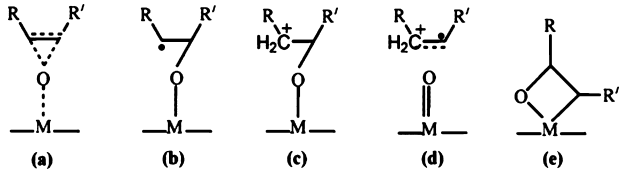

Scheme 4. Proposed Radical Intermediate During Epoxidation

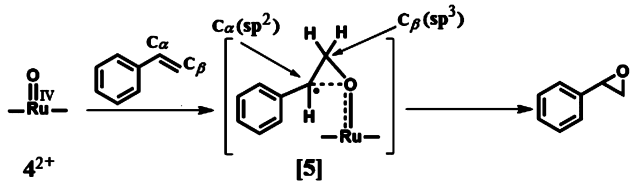

level for $\mathbf{1a}^{+}$−$\mathbf{1d}^{+}$, $\mathbf{1a}^{-}$−$\mathbf{1d}^{-}$, $\mathbf{2}^{+}$, $\mathbf{2}^{-}$, and $\mathbf{3a}^{2+}$ and (U)B3LYP level[35] for $\mathbf{1a}^{2+}$−$\mathbf{1d}^{2+}$, **1a**−**1d**, $\mathbf{1d}^{2-}$, $\mathbf{1d}^{3-}$, and $\mathbf{2}^{2+}$, and **2** used the Gaussian 09 program package.[36] Except ruthenium all other elements were assigned the 6-31G* basis set. The SDD (in $\mathbf{2}^{2+}$, $\mathbf{2}^{+}$, **2**, $\mathbf{2}^{-}$) and LANL2DZ (in $\mathbf{1a}^{2+}$−$\mathbf{1d}^{2+}$, $\mathbf{1a}^{+}$−$\mathbf{1d}^{+}$, **1a**−**1d**, $\mathbf{1a}^{-}$−$\mathbf{1d}^{-}$, $\mathbf{3a}^{2+}$) basis sets with effective core potential were employed for the ruthenium atom.[37] The vibrational frequency calculations were performed to ensure that the optimized geometries represent the local minima and there are only positive eigenvalues. All calculations were performed with the Gaussian09 program package. Vertical electronic excitations based on (R)B3LYP/(U)B3LYP-optimized geometries were computed for $\mathbf{1a}^{n}$−$\mathbf{1d}^{n}$ (n = +2, +1, 0) and $\mathbf{2}^{n}$ (n = +2, +1, 0) using the time-dependent density functional theory (TD-DFT) formalism[38] in acetonitrile using a conductor-like polarizable continuum model (CPCM).[39] Chemissian 1.7[40] was used to calculate the fractional contributions of various groups to each molecular orbital. All calculated structures were visualized with ChemCraft.[41]

General Procedure for Catalytic Epoxidation Studies. The catalyst [**1a**]ClO_4 (4.13 mg, 0.0049 mmol, 1 mol %) in 3 mL of CH_2Cl_2 was taken in a vial and stirred for ∼15 min at 298 K. The olefin (0.50 mmol) was then added to it with simultaneous stirring followed by the addition of iodobenzene diacetate (2 equivalents with respect to olefin) as the oxidant. The mixture was stirred at 298 K for 6 h. The reaction mixture was then diluted with water and extracted with ethyl acetate (10 mL) three times. The combined organic extracts were dried over Na_2SO_4 and concentrated under reduced pressure, and the yields were determined by gas chromatography with respect to the internal standard, *n*-decane (1 mmol). A 2.0 μL aliquot was subjected for analysis by GC-FID in each case.

Preparation of the Complexes. The complexes [**1a**]ClO_4−[**1d**]ClO_4 and [**2**]ClO_4 were synthesized by following a general procedure using respective R-BIAN. For [**2**]ClO_4 R-BIAN with R = H was used. The details are given below for [**1a**]ClO_4.

Synthesis of [Ru(tpm)(OMe-BIAN)Cl]ClO_4, [1a]ClO_4. Ru(tpm)-Cl_3·1.5 H_2O (101 mg, 0.24 mmol) and the ligand R-BIAN (R = OCH_3, Chart 2) (106 mg, 0.27 mmol) were taken in 40 mL of methanol. The reaction mixture was heated at reflux with stirring under a dinitrogen atmosphere for 8 h, and the color of the solution turned to reddish brown. The solvent was then evaporated under reduced pressure. The solid mass thus obtained was dissolved in 2 mL of acetonitrile followed by addition of a saturated aqueous solution of $NaClO_4$. The solution was then refrigerated for 6 h, and the resulting solid was filtered through a Buchner funnel and dried under vacuum. It was then purified on a neutral alumina column by using 4:1 CH_2Cl_2−CH_3CN as eluant. Evaporation of the solvent under reduced pressure yielded the solid product of [**1a**]ClO_4.

[**1a**]ClO_4: Yield 114 mg (57%). ^{1}H NMR in $CDCl_3$ [δ/ppm (J/Hz)]: 9.82 (s, 1H), 8.77 (d, 2.6, 1H), 8.36 (d, 2.4, 2H), 8.03 (d, 8.2, 2H), 7.70 (d, 7.2, 2H), 7.49 (t, 7.4, 2H), 7.24 (m,4H), 7.14 (d, 7.2, 2H), 6.99 (d, 2.1, 2H), 6.71 (d, 7.5, 2H), 6.47 (d, 2.6, 1H), 6.19 (t, 2.5, 3H), 3.80 (s, 6H). MS (ESI+, CH_3CN): m/z {$\mathbf{1a}^{+}$} calcd 743.122; found 743.128. IR (KBr): ν(ClO_4^-, cm^{-1}): 1093, 622. Molar conductivity (Λ_M (Ω^{-1} cm^2 M^{-1}), CH_3CN): 118. Anal. Calcd for $C_{36}H_{30}N_8Cl_2O_6Ru$: C, 51.31; H, 3.59; N, 13.30. Found: C, 51.31; H, 3.50; N, 13.18.

[**1b**]ClO_4: Yield 112 mg (58%). ^{1}H NMR in $CDCl_3$ [δ/ppm (J/Hz)]: 9.89 (s, 1H), 8.80 (d, 2.6, 1H), 8.38 (d, 2.6, 2H), 8.07 (d, 8.2, 2H), 7.78 (m, 2H), 7.52 (d, 7.8, 2H), 7.36 (m, 2H), 7.24 (m, 1H), 7.17 (d, 7.2, 2H), 7.00 (d, 1.6, 2H), 6.94 (m, 2H), 6.50 (t, 2.4, 1H), 6.30 (m, 2H), 6.23 (t, 2.4, 2H). MS (ESI+, CH_3CN): m/z {$\mathbf{1b}^{+}$} calcd 719.082; found 719.104. IR (KBr): ν(ClO_4^-, cm^{-1}): 1089, 622. Molar conductivity (Λ_M (Ω^{-1} cm^2 M^{-1}), CH_3CN): 114. Anal. Calcd for $C_{34}H_{24}N_8Cl_2F_2O_4Ru$: C, 49.89; H, 2.96; N, 13.69. Found: C, 49.74; H, 2.82; N, 13.23.

[**1c**]ClO_4: Yield 105 mg (52%). ^{1}H NMR in $CDCl_3$ [δ/ppm (J/Hz)]: 9.87 (s, 1H), 8.79 (d, 2.7, 1H), 8.37 (d, 2.6, 2H), 8.08 (d, 8.2, 2H), 7.74 (d, 6.6, 2H), 7.64 (d, 7.1, 2H), 7.52 (t, 8.1, 2H), 7.20 (m, 5H), 7.01 (d, 2.2, 2H), 6.51 (t, 2.6, 1H), 6.26 (d, 8.9, 1H), 6.24 (m, 3H). MS (ESI+, CH_3CN): m/z {$\mathbf{1c}^{+}$} calcd 751.023; found 751.060. IR (KBr): ν(ClO_4^-, cm^{-1}): 1086, 622. Molar conductivity (Λ_M (Ω^{-1} cm^2 M^{-1}), CH_3CN): 122. Anal. Calcd for $C_{34}H_{24}N_8Cl_4O_4Ru$: C, 47.96; H, 2.84; N, 13.16. Found: C, 48.12; H, 2.87; N, 13.04.

[**1d**]ClO_4: Yield 118 mg (57%). ^{1}H NMR in $CDCl_3$ [δ/ppm (J/Hz)]: 9.98 (s, 1H), 8.86 (d, 2.8, 1H), 8.57 (d, 8.3, 2H), 8.42 (d, 2.7, 2H), 8.15 (d, 8.2, 4H), 8.01 (d, 7.5, 2H), 7.56 (t, 7.8, 2H), 7.28 (d, 3.9, 1H), 7.12 (d, 7.2, 2H), 7.00 (d, 2.1, 2H), 6.57 (m, 1H), 6.50 (m, 2H), 6.23 (t, 2.6, 2H). MS (ESI+, CH_3CN): m/z {$\mathbf{1d}^{+}$} calcd 773.071; found 773.080. IR (KBr): ν(ClO_4^-, cm^{-1}): 1091, 622. Molar conductivity (Λ_M (Ω^{-1} cm^2 M^{-1}), CH_3CN): 108. Anal. Calcd for $C_{34}H_{24}N_{10}Cl_2O_8Ru$: C, 46.80; H, 2.77; N, 16.05. Found: C, 46.95; H, 2.80; N, 15.92.

[**2**]ClO_4: Yield 74 mg (44%). ^{1}H NMR in $CDCl_3$ [δ/ppm (J/Hz)]: 9.96 (s, 1H), 8.72 (d, 2.7, 1H), 8.56 (d, 2.1, 1H), 8.53 (d, 2.7, 1H), 8.42 (m, 1H), 8.41 (d, 1.8, 1H), 8.36 (d, 8.1, 1H), 8.18 (d, 8.2, 1H), 7.87 (t, 7.2, 2H), 7.53 (m, 6H), 6.97 (d, 2.1, 1H), 6.82 (d, 2.2, 1H), 6.68 (t, 2.5, 1H), 6.44 (t, 2.6, 1H), 6.14 (t, 2.6, 1H). MS (ESI+, CH_3CN): m/z {$\mathbf{2}^{+}$} calcd 608.053; found 608.037. IR (KBr): ν(ClO_4^-, cm^{-1}): 1090, 623; ν(C═O, cm^{-1}): 1690. Molar conductivity (Λ_M (Ω^{-1} cm^2 M^{-1}), CH_3CN): 92. Anal. Calcd for $C_{28}H_{21}Cl_2N_7O_5Ru$: C, 47.54; H, 2.99; N, 13.86. Found: C, 47.68; H, 2.80; N, 13.90.

Preparation of [Ru(tpm)(OMe-BIAN)(H_2O)](ClO_4)$_2$ ([3a]-(ClO_4)$_2$). The mixture of [**1a**]ClO_4 (100 mg, 0.12 mmol) and $AgClO_4$ (100 mg, 0.48 mmol) in 1:3 acetone−water (25 mL) was heated at reflux under stirring for 6 h. The initial reddish brown solution turned to yellow with the precipitation of AgCl. It was then cooled to room temperature and filtered through a sintered glass crucible (G4). The filtrate was concentrated to 5 mL under reduced pressure, and excess $NaClO_4$ was added to it. The solid [**3a**](ClO_4)$_2$

DOI: 10.1021/acs.inorgchem.5b00615
Inorg. Chem. 2015, 54, 4998−5012

thus obtained was filtered off and washed with a few drops of chilled Milli-Q water followed by drying in vacuo over P_4O_{10}.

[**3a**]$(ClO_4)_2$: Yield 80 mg (73%). ^{1}H NMR in D_2O [δ/ppm (J/Hz)]: 9.70 (s, 1H), 8.56 (d, 8.0, 1H), 8.46 (d, 3.0, 1H), 8.35 (d, 2.7, 1H), 8.19 (d, 6.0, 1H), 8.13 (d, 7.0, 1H), 7.89 (d, 2.1, 1H), 7.84 (d, 2.2, 1H), 7.53 (m, 2H), 7.16 (m, 8H), 6.70 (m, 1H), 6.61 (d, 3.0, 1H), 6.34 (m, 4H) 3.79 (s, 6H). MS (ESI+, CH_3OH): m/z {**3a**$(ClO_4)_2$−ClO_4−H_2O}$^+$ calcd 807.102; found 807.092. IR (KBr): ν(OH, cm^{-1}): 3438; ν(ClO_4^-, cm^{-1}): 1092, 623. Molar conductivity (Λ_M (Ω^{-1} cm^2 M^{-1}), H_2O): 195. Anal. Calcd for $C_{36}H_{32}N_8Cl_2O_{11}Ru$: C, 46.76; H, 3.49; N, 12.12. Found: C, 46.54; H, 3.21; N, 12.32.

Caution! Perchlorate salts of metal complexes with organic ligands are potentially explosive. Heating of dried samples must be avoided; handling of even a small amount has to proceed with great caution.

■ ASSOCIATED CONTENT

Supporting Information

X-ray crystallographic files in CIF format for [**1a**]ClO_4, [**2**]ClO_4, and [**3a**]$(PF_6)_2$, mass spectra, cyclic and differential pulse voltammograms of [**3a**]$(PF_6)_2$, electronic spectra, ^{1}H NMR, ^{31}P NMR spectra, DFT-optimized structures, bond parameters, MO compositions, and energies of DFT optimized states. The Supporting Information is available free of charge on the ACS Publications website at DOI: 10.1021/acs.inorgchem.5b00615.

■ AUTHOR INFORMATION

Corresponding Author

*E-mail: lahiri@chem.iitb.ac.in.

Notes

The authors declare no competing financial interest.

■ ACKNOWLEDGMENTS

Financial support received from the Department of Science and Technology, University Grants Commission (fellowship to A.H. and R.R.), Council of Scientific and Industrial Research (fellowship to A.D., H.A. and S.M.), New Delhi (India) is gratefully acknowledged.

■ REFERENCES

(1) (a) Argazzi, R.; Iha, N. Y. M.; Zabri, H.; Odobel, F.; Bignozzi, C. A. *Coord. Chem. Rev.* **2004**, *248*, 1299−1316. (b) Sun, L.; Hammarström, L.; Åkermark, B.; Styring, S. *Chem. Soc. Rev.* **2001**, *30*, 36−49. (c) Concepcion, J. J.; Jurss, J. W.; Brennaman, M. K.; Hoertz, P. G.; Patrocinio, A. O. T.; Iha, N. Y. M.; Templeton, J. L.; Meyer, T. J. *Acc. Chem. Res.* **2009**, *42*, 1954−1965. (d) Balzani, V.; Credi, A.; Venturi, M. *Chem. Soc. Rev.* **2009**, *38*, 1542−1550. (e) Balzani, V.; Credi, A.; Silvi, S.; Venturi, M. *Chem. Soc. Rev.* **2006**, *35*, 1135−1149. (f) Wolfbeis, O. S.; Klimant, I.; Werner, T.; Huber, C.; Kosch, U.; Krause, C.; Neurauter, G.; Dürkop, A. *Sens. Actuators, B* **1998**, *51*, 17−24. (g) Hurst, J. K. *Coord. Chem. Rev.* **2005**, *249*, 313−328. (h) Zhang, S.; Baldino, S.; Baratta, W. *Organometallics* **2013**, *32*, 5299−5304. (i) Ma, G.; McDonald, R.; Ferguson, M.; Cavell, R. G.; Patrick, B. O.; James, B. R.; Hu, T. Q. *Organometallics* **2013**, *26*, 846−854. (j) Barton, J. K.; Olmon, E. D.; Sontz, P. A. *Coord. Chem. Rev.* **2011**, *255*, 619−634. (k) Lim, M. H.; Song, H.; Olmon, E. D.; Dervan, E. E.; Barton, J. K. *Inorg. Chem.* **2009**, *48*, 5392−5397. (l) Puckett, C. A.; Barton, J. K. *Biochemistry* **2008**, *47*, 11711−11716. (m) Schulz, M.; Karnahl, M.; Schwalbe, M.; Vos, J. G. *Coord. Chem. Rev.* **2012**, *256*, 1682−1705. (n) Hoogenboom, R.; Schubert, U. S. *Chem. Soc. Rev.* **2006**, *35*, 622−629.

(2) (a) O'Brien, C.; Wong, M. Y.; Cordes, D. B.; Slawin, A. M. Z.; Zysman-Colman, E. *Organometallics* **2015**, *34*, 13−22. (b) Nunes, C. D.; Vaz, P. D.; Félix, V.; Veiros, L. F.; Moniz, T.; Rangel, M.; Realista, S.; Mourato, A. C.; Calhorda, M. J. *Dalton Trans.* **2015**, *44*, 5125−5138. (c) Schmitz, M.; Seibel, M.; Kelm, H.; Demeshko, S.; Meyer, F.; Krüger, H.-J. *Angew. Chem., Int. Ed.* **2014**, *53*, 5988−5992. (d) Tao, W.-J.; Li, J.-F.; Peng, A.-Q.; Sun, X. -L; Yang, X.-H.; Tang, Y. *Chem.—Eur. J.* **2013**, *19*, 13956−13961. (e) Fedushkin, I. L.; Sokolov, V. G.; Piskunov, A. V.; Makarov, V. M.; Baranov, E. V.; Abakumav, G. A. *Chem. Commun.* **2014**, *50*, 10108−10111. (f) Wen, C.; Yuan, S.; Shi, Q.; Yue, E.; Liu, D.; Sun, W.-H. *Organometallics* **2014**, *33*, 7223−7231. (g) Bridges, C. R.; McCormick, T. M.; Gibson, G. L.; Hollinger, J.; Seferos, D. S. *J. Am. Chem. Soc.* **2013**, *135*, 13212−13219. (h) Fedushkin, I. L.; Markina, O. V.; Lukoyanov, A. N.; Morozov, A. G.; Baranov, E. V.; Maslov, M. O.; Ketkov, S. Y. *Dalton Trans.* **2013**, *42*, 7952−7961. (i) Papanikolaou, P. A.; Gdaniec, M.; Wicher, B.; Akrivos, P. D.; Tkachenko, N. V. *Eur. J. Inorg. Chem.* **2013**, 5196−5205. (j) Fedushkin, I. L.; Maslova, O. V.; Morozov, A. G.; Dechert, S.; Demeshko, S.; Meyer, F. *Angew. Chem., Int. Ed.* **2012**, *51*, 10584−10587. (k) Li, L.; Lopes, P. S.; Rosa, V.; Figueira, C. A.; Lemos, M. A. N. D. A.; Duarte, M. T.; Avilés, T.; Gomes, P. T. *Dalton Trans.* **2012**, *41*, 5144−5154. (l) Clark, K. M.; Bendix, J.; Heyduk, A. F.; Ziller, J. W. *Inorg. Chem.* **2012**, *51*, 7457−7459. (m) Hill, N. J.; Vargas-Baca, I.; Cowley, A. H. *Dalton Trans.* **2009**, 240−253. (n) Fedushkin, I. L.; Skatova, A. A.; Chudakova, V. A.; Fukin, G. K. *Angew. Chem., Int. Ed.* **2003**, *42*, 3294−3298. (o) van Asselt, R.; Elsevier, C. J.; Smeets, W. J. J.; Spek, A. L. *Inorg. Chem.* **1994**, *33*, 1521−1531.

(3) (a) Mondal, P.; Agarwala, H.; Jana, R. D.; Plebst, S.; Grupp, A.; Ehret, F.; Mobin, S. M.; Kaim, W.; Lahiri, G. K. *Inorg. Chem.* **2014**, *53*, 7389−7403. (b) Ragaini, F.; Cenini, S.; Borsani, E.; Dompé, M.; Gallo, E. *Organometallics* **2001**, *20*, 3390−3398. (c) Singh, S. K.; Dubey, S. K.; Pandey, R.; Mishra, L.; Zou, R.-Q; Xu, Q.; Pandey, D. K. *Polyhedron* **2008**, *27*, 2877−2882. (d) Viganó, M.; Ragaini, F.; Buonomenna, M. G.; Lariccia, R.; Caselli, A.; Gallo, E.; Cenini, S.; Jansen, J. C.; Drioli, E. *ChemCatChem* **2010**, *2*, 1150−1164.

(4) (a) Crawford, K.; Rautenstrauch, V.; Uijttewaal, A. *Synlett* **2001**, 1127−1128. (b) Wahren, U.; Sprung, I.; Schulze, K.; Findeisen, M.; Buchbauer, G. *Tetrahedron Lett.* **1999**, *40*, 5991−5992. (c) Kelly, D. R.; Nally, J. *Tetrahedron Lett.* **1999**, *40*, 3251−3254.

(5) (a) Grigoropoulou, G.; Clark, J. H.; Elings, J. A. *Green Chem.* **2003**, *5*, 1−7. (b) Lane, B. S.; Burgess, K. *Chem. Rev.* **2003**, *103*, 2457−2473. (c) Beller, M. *Adv. Synth. Catal.* **2004**, *346*, 107−108. (d) Legros, J.; Bolm, C. *Chem.—Eur. J.* **2005**, *11*, 1086−1092. (e) Bregeault, J. M. *Dalton Trans.* **2003**, 3289−3302. (f) Herrmann, W. A.; Fischer, R. W.; Marz, D. W. *Angew. Chem., Int. Ed.* **1991**, *30*, 1638−1641. (g) Rudolf, J.; Reddy, K. L.; Chiang, J. P.; Sharpless, K. B. *J. Am. Chem. Soc.* **1997**, *119*, 6189−6190. (h) Hermann, W. A.; Kratzer, R. M.; Ding, H.; Thiel, W. R.; Glas, H. *J. Organomet. Chem.* **1998**, *555*, 293−295. (i) Shi, Y. *Acc. Chem. Res.* **2004**, *37*, 488−496. (j) Gerlach, A.; Geller, T. *Adv. Synth. Catal.* **2004**, *346*, 1247−1249. (k) Yang, D. *Acc. Chem. Res.* **2004**, *37*, 497−505.

(6) Nishiyama, H.; Shimada, T.; Itoh, H.; Sugiyama, H.; Motoyama, Y. *Chem. Commun.* **1997**, 1863−1864.

(7) (a) Dakkach, M.; López, M. I.; Romero, I.; Rodríguez, M.; Atlamsani, A.; Parella, T.; Fontrodona, X.; Llobet, A. *Inorg. Chem.* **2010**, *49*, 7072−7079. (b) Chatterjee, D. *Inorg. Chim. Acta* **2008**, *361*, 2177−2182. (c) Chatterjee, D.; Sengupta, A.; Mitra, A. *Polyhedron* **2007**, *26*, 178−183. (d) Benet-Buchholz, J.; Comba, P.; Llobet, A.; Roeser, S.; Vadivelu, P.; Wadepohl, H.; Wiesner, S. *Dalton Trans.* **2009**, 5910−5923. (e) Tse, M. K.; Döbler, C.; Bhor, S.; Klawonn, M.; Mägerlein, W.; Hugl, H.; Beller, M. *Angew. Chem., Int. Ed.* **2004**, *43*, 5255−5260. (f) Tse, M. K.; Bhor, S.; Klawonn, M.; Anilkumar, G.; Jiao, H.; Spannenberg, A.; Döbler, C.; Mägerlein, W.; Hugl, H.; Beller, M. *Chem.—Eur. J.* **2006**, *12*, 1875−1888. (g) Tse, M. K.; Klawonn, M.; Bhor, S.; Döbler, C.; Anilkumar, G.; Hugl, H.; Mägerlein, W.; Beller, M. *Org. Lett.* **2005**, *7*, 987−990. (h) Schröder, K.; Enthaler, S.; Join, B.; Junge, K.; Beller, M. *Adv. Synth. Catal.* **2010**, *352*, 1771−1778.

(8) (a) Mariappan, K.; Alaparthi, M.; Caple, G.; Balasubramanian, V.; Hoffman, M. M.; Hudspeth, M.; Sykes, A. G. *Inorg. Chem.* **2014**, *53*, 2953−2962. (b) Marcazzan, P.; Abu-Gnim, C.; Seneviratne, K. N.; James, B. R. *Inorg. Chem.* **2004**, *43*, 4820−4824. (c) Chanda, N.; Mondal, B.; Puranik, V. G.; Lahiri, G. K. *Polyhedron* **2002**, *21*, 2033−2043.

DOI: 10.1021/acs.inorgchem.5b00615
Inorg. Chem. 2015, 54, 4998−5012

(9) Visentin, L. C.; Ferreira, L. C.; Bordinhão, J.; Filgueiras, C. A. L. *J. Braz. Chem. Soc.* **2010**, *21*, 1187−1194.
(10) Anga, S.; Paul, M.; Naktode, K.; Kottalanka, R. K.; Panda, T. K. *Z. Anorg. Allg. Chem.* **2012**, *638*, 1311−1315.
(11) Anga, S.; Rej, S.; Naktode, K.; Pal, T.; Panda, T. K. *J. Chem. Sci.* **2015**, *127*, 103−113.
(12) (a) Liu, Y.; Ng, S.-M.; Yiu, S.-M.; Lam, W. W. Y.; Wei, X.-G.; Lau, K.-C.; Lau, T.-C. *Angew. Chem., Int. Ed.* **2014**, *53*, 14468−14471. (b) Rilak, A.; Bratsos, I.; Zangrando, E.; Kljun, J.; Turel, I.; Bugarčić, Ž. D.; Alessio, E. *Inorg. Chem.* **2014**, *53*, 6113−6126.
(13) (a) Agarwala, H.; Ehret, F.; Chowdhury, A. D.; Maji, S.; Mobin, S. M.; Kaim, W.; Lahiri, G. K. *Dalton Trans.* **2013**, *42*, 3721−3734. (b) Serrano, I.; López, M. I.; Ferrer, Í.; Poater, A.; Parella, T.; Fontrodona, X.; Solà, M.; Llobet, A.; Rodríguez, M.; Romero, I. *Inorg. Chem.* **2011**, *50*, 6044−6054. (c) Yoshida, M.; Masaoka, S.; Abe, J.; Sakai, K. *Chem.—Asian J.* **2010**, *5*, 2369−2378.
(14) Farrugia, L. J. *J. Appl. Crystallogr.* **2012**, *45*, 849−854.
(15) (a) Du, W.; Wang, Q.; Wang, L.; Yu, Z. *Organometallics* **2014**, *33*, 974−982. (b) Das, A.; Scherer, T. M.; Chowdhury, A. D.; Mobin, S. M.; Kaim, W.; Lahiri, G. K. *Inorg. Chem.* **2012**, *51*, 1675−1684.
(16) (a) Sala, X.; Romero, I.; Rodríguez, M.; Escriche, L.; Llobet, A. *Angew. Chem., Int. Ed.* **2009**, *48*, 2842−2852. (b) Tseng, H.-W.; Zong, R.; Muckerman, J. T.; Thummel, R. *Inorg. Chem.* **2008**, *47*, 11763−11773.
(17) Bag, N.; Lahiri, G. K.; Bhattacharya, S.; Falvello, L. R.; Chakravorty, A. *Inorg. Chem.* **1988**, *27*, 4396−4402.
(18) Takeuchi, K. J.; Thompson, M. S.; Pipes, D. W.; Meyer, T. J. *Inorg. Chem.* **1988**, *23*, 1845−1851.
(19) Jones, W. E., Jr.; Bignozzi, C. A.; Chen, P.; Meyer, T. J. *Inorg. Chem.* **1993**, *32*, 1167−1178.
(20) Serrano, I.; Sala, X.; Plantalech, E.; Rodríguez, M.; Romero, I.; Jansat, S.; Gómez, M.; Parella, T.; Stoeckli-Evans, H.; Solans, X.; Font-Bardia, M.; Vidjayacoumar, B.; Llobet, A. *Inorg. Chem.* **2007**, *46*, 5381−5389.
(21) De, P.; Mondal, T. K.; Mobin, S. M.; Lahiri, G. K. *Inorg. Chim. Acta* **2011**, *372*, 250−258.
(22) (a) Patra, S.; Sarkar, B.; Mobin, S. M.; Kaim, W.; Lahiri, G. K. *Inorg. Chem.* **2003**, *42*, 6469−6473. (b) Kundu, T.; Mobin, S. M.; Lahiri, G. K. *Dalton Trans.* **2010**, *39*, 4232−4242. (c) Mandal, A.; Kundu, T.; Ehret, F.; Bubrin, M.; Mobin, S. M.; Kaim, W.; Lahiri, G. K. *Dalton Trans.* **2014**, *43*, 2473−2487. (d) Ghosh, P.; Mondal, P.; Ray, R.; Das, A.; Bag, S.; Mobin, S. M.; Lahiri, G. K. *Inorg. Chem.* **2014**, *53*, 6094−6106.
(23) Patra, S.; Sarkar, B.; Ghumaan, S.; Patil, M. P.; Mobin, S. M.; Sunoj, R. B.; Kaim, W.; Lahiri, G. K. *Dalton Trans.* **2005**, 1188−1194.
(24) (a) Chowdhury, A. D.; Das, A.; Irshad, K.; Mobin, S. M.; Lahiri, G. K. *Inorg. Chem.* **2011**, *50*, 1775−1785. (b) Chanda, N.; Mobin, S. M.; Puranik, V. G.; Niemeyer, M.; Datta, A.; Lahiri, G. K. *Inorg. Chem.* **2004**, *43*, 1056−1064. (c) Maji, S.; López, I.; Bozoglian, F.; Benet-Buchholz, J.; Llobet, A. *Inorg. Chem.* **2013**, *52*, 3591−3593. (d) Badiei, Y. M.; Polyansky, D. E.; Muckerman, J. T.; Szalda, D. J.; Haberdar, R.; Zong, R.; Thummel, R. P.; Fujita, E. *Inorg. Chem.* **2013**, *52*, 8845−8850. (e) Neudeck, S.; Maji, S.; López, I.; Meyer, S.; Meyer, F.; Llobet, A. *J. Am. Chem. Soc.* **2014**, *136*, 24−27. (f) Vaquer, L.; Miró, P.; Sala, X.; Bozoglian, F.; Masllorens, E.; Benet-Buchholz, J.; Fontrodona, X.; Parella, T.; Romero, I.; Roglans, A.; Rodríguez, M.; Bo, C.; Llobet, A. *ChemPlusChem* **2013**, *78*, 235−243. (g) Ohzu, S.; Ishizuka, T.; Hirai, Y.; Jiang, H.; Sakaguchi, M.; Ogura, T.; Fukuzumi, S.; Kojima, T. *Chem. Sci.* **2012**, *3*, 3421−3431.
(25) Juris, A.; Balzani, V.; Barigelletti, F.; Campagna, S.; Belser, P.; von Zelewsky, A. *Coord. Chem. Rev.* **1988**, *84*, 85−277.
(26) (a) Pappo, R.; Allen, D. S., Jr.; Lemieux, R. U.; Johnson, W. S. *J. Org. Chem.* **1956**, *21*, 478−479. (b) Carlsen, P. H. J.; Katsuki, T.; Martin, V. S.; Sharpless, K. B. *J. Org. Chem.* **1981**, *46*, 3936−3938. (c) Das, A.; Ghosh, T. K.; Chowdhury, A. D.; Mobin, S. M.; Lahiri, G. K. *Polyhedron* **2013**, *52*, 1130−1137.
(27) (a) Paull, D. E.; Keagy, B. A.; Kron, E. J.; Wilcox, B. R. *J. Surg. Res.* **1989**, *46*, 333−338. (b) Bunda, S.; Kaviani, N.; Hinek, A. *J. Biol. Chem.* **2005**, *280*, 2341−2351.
(28) (a) Acquaye, J. H.; Muller, J. G.; Takeuchi, K. J. *Inorg. Chem.* **1993**, *32*, 160−165. (b) Lai, S.; Lepage, C. J.; Lee, D. G. *Inorg. Chem.* **2002**, *41*, 1954−1957. (c) Hamelin, O.; Ménage, S.; Charnay, F.; Chavarot, M.; Pierre, J.-L.; Pécaut, J.; Fontecave, M. *Inorg. Chem.* **2008**, *47*, 6413−6420. (d) Chavarot, M.; Ménage, S.; Hamelin, O.; Charnay, F.; Pécaut, J.; Fontecave, M. *Inorg. Chem.* **2003**, *42*, 4810−4816.
(29) (a) Groves, J. T.; Kruper, W. J. *J. Am. Chem. Soc.* **1979**, *101*, 7613−7615. (b) Groves, J. T.; Nemo, T. E. *J. Am. Chem. Soc.* **1983**, *105*, 5786−5791. (c) Jørgensen, K. A. *Chem. Rev.* **1989**, *89*, 431−458. (d) Meunier, B. *Chem. Rev.* **1992**, *92*, 1411−1456. (e) Jørgensen, K. A.; Schiøtt, B. *Chem. Rev.* **1990**, *90*, 1483−1506. (f) Ostovic, D.; Bruice, T. C. *Acc. Chem. Res.* **1992**, *25*, 314−320. (g) Fung, W.-H.; Yu, W.-Y.; Che, C.-M. *J. Org. Chem.* **1998**, *63*, 7715−7726.
(30) Reger, D. L.; Grattan, T. C.; Brown, K. J.; Little, C. A.; Lamba, J. J. S.; Rheingold, A. L.; Sommer, R. D. *J. Organomet. Chem.* **2000**, *607*, 120−128.
(31) (a) Mak, C. S. K.; Wong, H. L.; Leung, Q. Y.; Tam, W. Y.; Chan, W. K.; Djurišic, A. B. *J. Organomet. Chem.* **2009**, *694*, 2770. (b) Gasperini, M.; Ragaini, F.; Cenini, S. *Organometallics* **2002**, *21*, 2950−2957.
(32) Llobet, A.; Doppelt, P.; Meyer, T. J. *Inorg. Chem.* **1988**, *27*, 514−520.
(33) (a) Sheldrick, G. M. *Acta Crystallogr., Sect. A* **2008**, *A64*, 112−122. (b) *Program for Crystal Structure Solution and Refinement*; University of Göttingen: Göttingen, Germany, 1997.
(34) Sluis, P. V. D.; Spek, A. L. *Acta Crystallogr., Sect. A* **1990**, *46*, 194−201.
(35) Lee, C.; Yang, W.; Parr, R. G. *Phys. Rev. B* **1998**, *37*, 785−789.
(36) Frisch, M. J.; Trucks, G. W.; Schlegel, H. B.; Scuseria, G. E.; Robb, M. A.; Cheeseman, J. R.; Scalmani, G.; Barone, V.; Mennucci, B.; Petersson, G. A.; Nakatsuji, H.; Caricato, M.; Li, X.; Hratchian, H. P.; Izmaylov, A. F.; Bloino, J.; Zheng, G.; Sonnenberg, J. L.; Hada, M.; Ehara, M.; Toyota, K.; Fukuda, R.; Hasegawa, J.; Ishida, M.; Nakajima, T.; Honda, Y.; Kitao, O.; Nakai, H.; Vreven, T.; Montgomery, J. A.; Peralta, Jr. J. E.; Ogliaro, F.; Bearpark, M.; Heyd, J. J.; Brothers, E.; Kudin, K. N.; Staroverov, V. N.; Kobayashi, R.; Normand, J.; Raghavachari, K.; Rendell, A.; Burant, J. C.; Iyengar, S. S.; Tomasi, J.; Cossi, M.; Rega, N.; Millam, J. M.; Klene, M.; Knox, J. E.; Cross, J. B.; Bakken, V.; Adamo, C.; Jaramillo, J.; Gomperts, R.; Stratmann, R. E.; Yazyev, O.; Austin, A. J.; Cammi, R.; Pomelli, C.; Ochterski, J. W.; Martin, R. L.; Morokuma, K.; Zakrzewski, V. G.; Voth, G. A.; Salvador, P.; Dannenberg, J. J.; Dapprich, S.; Daniels, A. D.; Farkas, O.; Foresman, J. B.; Ortiz, J. V.; Cioslowski, J.; Fox, D. J. *Gaussian 09*, Revision A.02: Gaussian, Inc.: Wallingford CT, 2009.
(37) (a) Andrae, D.; Haeussermann, U.; Dolg, M.; Stoll, H.; Preuss, H. *Theor. Chim. Acta* **1990**, *77*, 123−141. (b) Fuentealba, P.; Preuss, H.; Stoll, H.; Szentpaly, L. V. *Chem. Phys. Lett.* **1989**, *89*, 418−422.
(38) (a) Bauernschmitt, R.; Ahlrichs, R. *Chem. Phys. Lett.* **1996**, *256*, 454−464. (b) Stratmann, R. E.; Scuseria, G. E.; Frisch, M. J. *J. Chem. Phys.* **1998**, *109*, 8218−8225. (c) Casida, M. E.; Jamorski, C.; Casida, K. C.; Salahub, D. R. *J. Chem. Phys.* **1998**, *108*, 4439−4450.
(39) (a) Barone, V.; Cossi, M. *J. Phys. Chem. A* **1998**, *102*, 1995−2001. (b) Cossi, M.; Barone, V. *J. Chem. Phys.* **2001**, *115*, 4708−4718. (c) Cossi, M.; Rega, N.; Scalmani, G.; Barone, V. *J. Comput. Chem.* **2003**, *24*, 669−681.
(40) O'Boyle, N. M.; Tenderholt, A. L.; Langner, K. M. *J. Comput. Chem.* **2008**, *29*, 839−845.
(41) Zhurko, D. A.; Zhurko, G. A. *ChemCraft 1.5*; Plimus: San Diego, CA. Available at http://www.chemcraftprog.com.

DOI: 10.1021/acs.inorgchem.5b00615
Inorg. Chem. 2015, 54, 4998−5012